

1 **Measurement report: Long-term measurements of aerosol precursor concentrations in the Finnish sub-**  
2 **Arctic boreal forest**

3 Tuija Jokinen<sup>1,2\*</sup>, Katrianne Lehtipalo<sup>1,3</sup>, Roseline Cutting Thakur<sup>1</sup>, Ilona Ylivinkka<sup>1</sup>, Kimmo Neitola<sup>1</sup>, Nina  
4 Sarnela<sup>1</sup>, Totti Laitinen<sup>1</sup>, Markku Kulmala<sup>1</sup>, Tuukka Petäjä<sup>1</sup> and Mikko Sipilä<sup>1</sup>

5 <sup>1</sup>Institute for Atmospheric and Earth System Research (INAR) / Physics, Faculty of Science, University of  
6 Helsinki, P.O. Box 64, Helsinki, 00014 University of Helsinki

7 <sup>2</sup>Climate & Atmosphere Research Centre (CARE-C), The Cyprus Institute, P.O. Box 27456, Nicosia, CY-  
8 1645, Cyprus

9 <sup>3</sup>Finnish Meteorological Institute, Helsinki, Finland

10 \*correspondence to [t.jokinen@cyi.ac.cy](mailto:t.jokinen@cyi.ac.cy)

11

12 **Abstract:**

13 Aerosol particles form in the atmosphere by clustering of certain atmospheric vapors. After growing to larger  
14 particles by condensation of low volatile gases, they can affect the Earth's climate by scattering light and by  
15 acting as cloud condensation nuclei. Observations of low-volatility aerosol precursor gases have been reported  
16 around the world but longer-term measurement series and any Arctic data sets showing seasonal variation are  
17 close to non-existent. In here, we present ~7 months of aerosol precursor gas measurements performed with  
18 the nitrate based chemical ionization mass spectrometer (CI-APi-TOF). We deployed our measurements ~150  
19 km North of the Arctic Circle at the continental Finnish sub-Arctic field station, SMEAR I, located in Värriö  
20 strict nature reserve. We report concentration measurements of the most common new particle formation  
21 related compounds; sulfuric acid (SA), methane sulfonic acid (MSA), iodic acid (IA) and a total concentration  
22 of highly oxygenated organic compounds (HOMs). At this remote measurement site, SA is originated both  
23 from anthropogenic and biological sources and has a clear diurnal cycle but no significant seasonal variation.  
24 MSA shows a more distinct seasonal cycle with concentrations peaking in the summer. Of the measured  
25 compounds, iodic acid concentrations are the most stable throughout the measurement period, except in April,  
26 when the concentration of IA is significantly higher than during the rest of the year. Otherwise, IA has almost  
27 identical daily maximum concentrations in spring, summer and autumn, and on new particle formation event  
28 or non-event days. HOMs are abundant during the summer months and low in the autumn months. Due to the  
29 low autumn concentrations and their high correlation with ambient air temperature, we suggest that most of  
30 HOMs are products of biogenic emissions, most probably monoterpene oxidation products. New particle  
31 formation events at SMEAR I happen under relatively low temperatures (1 – 8 °C) with a fast temperature rise  
32 in the early morning hours, lower and decreasing RH (55% vs. 80%) during the NPF days compared to non-  
33 event days. NPF days have clearly higher global irradiance values (~450 m<sup>-2</sup> vs. ~200 m<sup>-2</sup>) and about 10 ppbv  
34 higher ozone concentrations than non-event days. During NPF days, we have on average higher SA  
35 concentration peaking at noon, higher MSA concentrations in the afternoon and slightly higher IA  
36 concentration than during non-event days. All together, these are the first long term measurements of aerosol  
37 forming vapors from the SMEAR I in the sub-arctic region, and the results help us to understand atmospheric  
38 chemical processes and aerosol formation in the rapidly changing Arctic.

39 **1. Introduction:**

40 The climate of sub-Arctic region is characterized with some of the most extreme temperature variations on  
41 Earth. We expect that during the course of the 21<sup>st</sup> century, the boreal forest is to experience the largest increase  
42 in temperatures of all forest biomes (IPCC, 2013), making it the most vulnerable to climate change. The boreal  
43 forest (taiga) covers most of the sub-Arctic and encompasses more than 30% of all forests on Earth, being one  
44 of the largest biome in the world (Brandt et al., 2013). The expected rate of changes, may overwhelm the  
45 resilience of forest ecosystems and possibly lead to significant biome-level changes (Reyer et al., 2015). The

46 forest-atmosphere systems are closely interlinked to one another. The forest stores carbon and water in the  
47 peat, soil and as biomass while at the same time vegetation emits volatile organic compounds (VOC) into the  
48 atmosphere (Bradshaw and Warkentin, 2015). In the Arctic, summer is short, but solar radiation is abundant  
49 and extends the daylight hours all the way to midnight and beyond. On the other hand, during the polar night  
50 air pollutants accumulate in the atmosphere due to cold and stable atmosphere, while turbulent mixing is  
51 inhibited, and the lack of removal processes lead to the formation of Arctic haze (Stohl, 2006). These features  
52 make the Arctic an interesting study region for photochemistry of reduced atmospheric compounds. Oxidation  
53 processes that dominantly occur in the summer time control the processes removing VOCs and other traces  
54 gases, such as SO<sub>2</sub> and NO<sub>x</sub>, from the atmosphere in the Arctic. Detailed understanding of atmospheric  
55 processes leading to aerosol precursor formation and gas-to-particle conversion and their role in feedback  
56 mechanisms help in assessing the future climate.

57 Aerosol and trace gas measurements in the sub-Arctic field station SMEAR I, go back to the 90s (Ahonen et  
58 al., 1997; Kulmala et al., 1998; Mäkelä et al., 1997). Trace gas and aerosol measurements at SMEAR I started  
59 in 1992 making them one of the longest continuous measurements of aerosol particle number and size  
60 distributions in the sub-Arctic (Ruuskanen et al., 2003). These long-term measurements show that aerosol  
61 particles regularly form and grow from very small sizes (< 8 nm diameter) with the highest frequency in the  
62 spring, between March and May (Dal Maso et al., 2007; Vehkamäki et al., 2004). It is suggested, that spring  
63 promotes new particle formation (NPF) because of the awakening of biological processes after the winter. At  
64 SMEAR I the snow only melts away in May-June and thus, many biological processes (photosynthesis)  
65 activate while the snow is still deep. This makes the Arctic spring a very complex environment for atmospheric  
66 chemistry with possible emission sources from melting snow, ice, melt water, vegetation and transport from  
67 other areas. At SMEAR I, most of the observed NPF events are either connected to clean air arriving from the  
68 Northern sector (originating from The Arctic Ocean and transported over boreal forest, Dal Maso et al., 2007)  
69 or the polluted air masses from the Eastern sector (Kyrö et al., 2014; Sipilä et al., 2021). Annually, around 30-  
70 60 NPF events are recorded at SMEAR I, of which around half could be initiated by anthropogenic air  
71 pollutants from the Kola Peninsula (Kyrö et al., 2014; Pirjola et al., 1998; Sipilä et al., 2021) leaving half of  
72 the events occurring from natural sources. The trend of NPF occurrence in Värriö is decreasing, as the  
73 anthropogenic sulfur dioxide emissions are decreasing in Russia (Kyrö et al., 2014).

74 Formation and growth of new particles at SMEAR I usually happen during daylight, highlighting the  
75 importance of photochemical activities. However, unlike most other locations, NPF is also observed during  
76 nighttime or polar night (Kyrö et al., 2014; Vehkamäki et al., 2004). Formation and growth processes of  
77 aerosols seem not to be correlated with each other at SMEAR I (Vehkamäki et al., 2004). Earlier literature  
78 reports, that the formation rate (J) has no clear seasonal trend, while the growth rates (GR) of small particles  
79 clearly peak during summer (Ruuskanen et al., 2007). This indicates that different chemistry drives the initial  
80 cluster formation and the subsequent growth processes. From the observed nucleation rates it has been  
81 proposed that NPF at SMEAR I could be due to sulfuric acid –ammonia (-water) nucleation (Napari et al.,  
82 2002) likely dominated by ion-induced channel at least during winter months (Sipilä et al., 2021). Kyrö et al.,  
83 2014 concludes that 20-50% of the condensational growth can also be explained by sulfuric acid in Värriö.  
84 Other studies speculate about the possibility of different organic compounds participating in NPF in the sub-  
85 Arctic. Tunved et al., 2006 studied the air masses arriving to SMEAR I and concluded that the aerosol mass  
86 increased linearly with time that the air masses travelled over land. The concentration of condensing gases  
87 over the boreal forest was concluded to be high and most likely consisting mainly of oxidation products of  
88 terpenes (VOCs) that are emitted by the forest. At SMEAR II station in Hyytiälä, approximately 700 km South-  
89 West of Värriö, oxidized organics mostly explain the growth of newly formed particles (Bianchi et al., 2017;  
90 Ehn et al., 2014). However, direct measurements of the aerosol forming and growing vapor species are still  
91 lacking from SMEAR I except during wintertime without biogenic activity when sulfuric acid has been shown  
92 to be primarily responsible on formation and growth (Sipilä et al., 2021). In Värriö, the role of NPF is critical  
93 in forming of cloud condensation nuclei (CCN), since measurements show that the number of CCN can  
94 increase up to 800 % as a result of NPF (Kerminen et al., 2012). In other locations in the boreal forest and  
95 Arctic, some measurements shed light into the possible chemical components that could be forming particles

96 in Värriö. Currently, the closest continuous measurements with the nitrate based CI-APi-TOF are conducted  
97 in Hyytiälä at the SMEAR II-station (Jokinen et al., 2012, 2017; Kulmala et al., 2013). In Hyytiälä there is  
98 direct evidence on the key role of the photochemical production of sulfuric acid and HOMs maintaining  
99 atmospheric NPF (Bianchi et al., 2017; Ehn et al., 2014; Jokinen et al., 2017; Kulmala et al., 2013).

100 Other chemical composition measurements of aerosol precursors have been conducted only in a few locations  
101 in the High-Arctic and over the Arctic Ocean (Baccarini et al., 2020; Beck et al., 2021; He et al., 2021; Sipilä  
102 et al., 2016). These studies show that in the Arctic, the marginal ice zone and the coast of the Arctic Ocean is  
103 a source of atmospheric iodic acid that is efficiently forming new particles. Sulfuric acid and MSA  
104 concentrations were also reported (Beck et al., 2021), but they were much lower in concentration than iodic  
105 acid (Baccarini et al., 2020). However, the chemistry behind NPF is not that simple, even in the pristine Arctic  
106 air. The clean air above the Arctic Ocean is abundant in dimethyl sulfide (DMS) emitted by phytoplankton,  
107 that rapidly oxidizes into sulfuric acid and MSA on sunny days and consequently forms cloud condensation  
108 nuclei (Charlson et al., 1987; Park et al., 2018). Beck et al., (2021) report, that in Svalbard in the Arctic Ocean,  
109 sulfuric acid and methane sulfonic acid contribute to the formation of secondary aerosol. They also observed  
110 that these compounds formed particles large enough to contribute to some extent to cloud condensation nuclei  
111 (CCN). This is supported by measurements of aerosol chemical composition from the Arctic that commonly  
112 report MSA in particulate matter (Dall'Osto et al., 2018; Kerminen et al., 1997). According to Beck et al.  
113 (2021) the initial aerosol formation in the high Arctic occurs via ion-induced nucleation of sulfuric acid and  
114 ammonia and subsequent growth by mainly sulfuric acid and MSA condensation during springtime and highly  
115 oxygenated organic molecules (HOM) during summertime. By contrast, in an ice-covered region around  
116 Villum, Greenland, Beck et al. (2021) observed new particle formation driven by iodic acid, but the particles  
117 remained small and did not grow to CCN sizes due to insufficient concentration of condensing vapors. Since  
118 the Arctic CCN number concentrations are low in general, formation of new particles is a very sensitive process  
119 affecting the composition of the aerosol population and CCN numbers in the area.

120 In this article, we present the measurements of aerosol precursor molecules from the continental SMEAR I  
121 station, ~150 km North of the Arctic Circle and ~150 km from the Arctic Ocean. We measured sulfuric acid,  
122 methane sulfonic acid, iodic acid and highly oxygenated organic compound concentrations with a sulfuric acid  
123 calibrated CI-APi-TOF (Jokinen et al., 2012; Kürten et al., 2012) to determine their levels in the sub-Arctic  
124 boreal forest and to understand whether these species are connected with the aerosol formation process in the  
125 area.

## 126 **2. Methods, measurement site and instrumentation:**

127 The core of this work is measurements of gas phase aerosol precursors. We use the nitrate chemical ionization  
128 atmospheric pressure interface time-of-flight mass spectrometer (CI-APi-ToF) that has been operational at the  
129 SMEAR I-station (N67°46, E29°36) in Eastern-Lapland since the early spring of 2019. SMEAR stands for  
130 Station for Measuring Ecosystem – Atmosphere Relations. Measurements were done on top of Kotovaara hill  
131 (390 m a.s.l.), close to ground level in an air-conditioned small log wood cottage. The cottage is surrounded  
132 by ~65-year-old Scotts pine forest. More details about the station can be found in earlier publications (Hari et  
133 al., 1994; Kyrö et al., 2014). The mass spectrometric measurements are designed to start a long-term  
134 measurement series of atmospheric aerosol forming trace gases in the Finnish Lapland and the measurements  
135 are ongoing to this day. We measure e.g. sulfuric acid, iodic acid, highly oxygenated organic molecules and  
136 methane sulfonic acid with high time resolution and precision. The measurements are running in Finnish winter  
137 time (UTC+2) throughout the year.

138 We calibrated the CI-APi-TOF twice during the measurement period and run the instrument with the same  
139 settings for the whole measurement period reported in this paper. We calibrated the instrument using a sulfuric  
140 acid calibrator described in Kürten et al., 2012. The calibration factor from the two separate calibrations were  
141 1)  $7 \cdot 10^9$  and 2)  $8 \cdot 10^9$  and we use the average  $7.5 \cdot 10^9$  in our study calculate the concentrations of all reported  
142 compounds. This factor includes the loss parameter due to the ~1 m long unheated inlet tube (3/4" stainless  
143 steel). HOMs and iodic acid have been estimated to be charged similarly at the kinetic limit as sulfuric acid

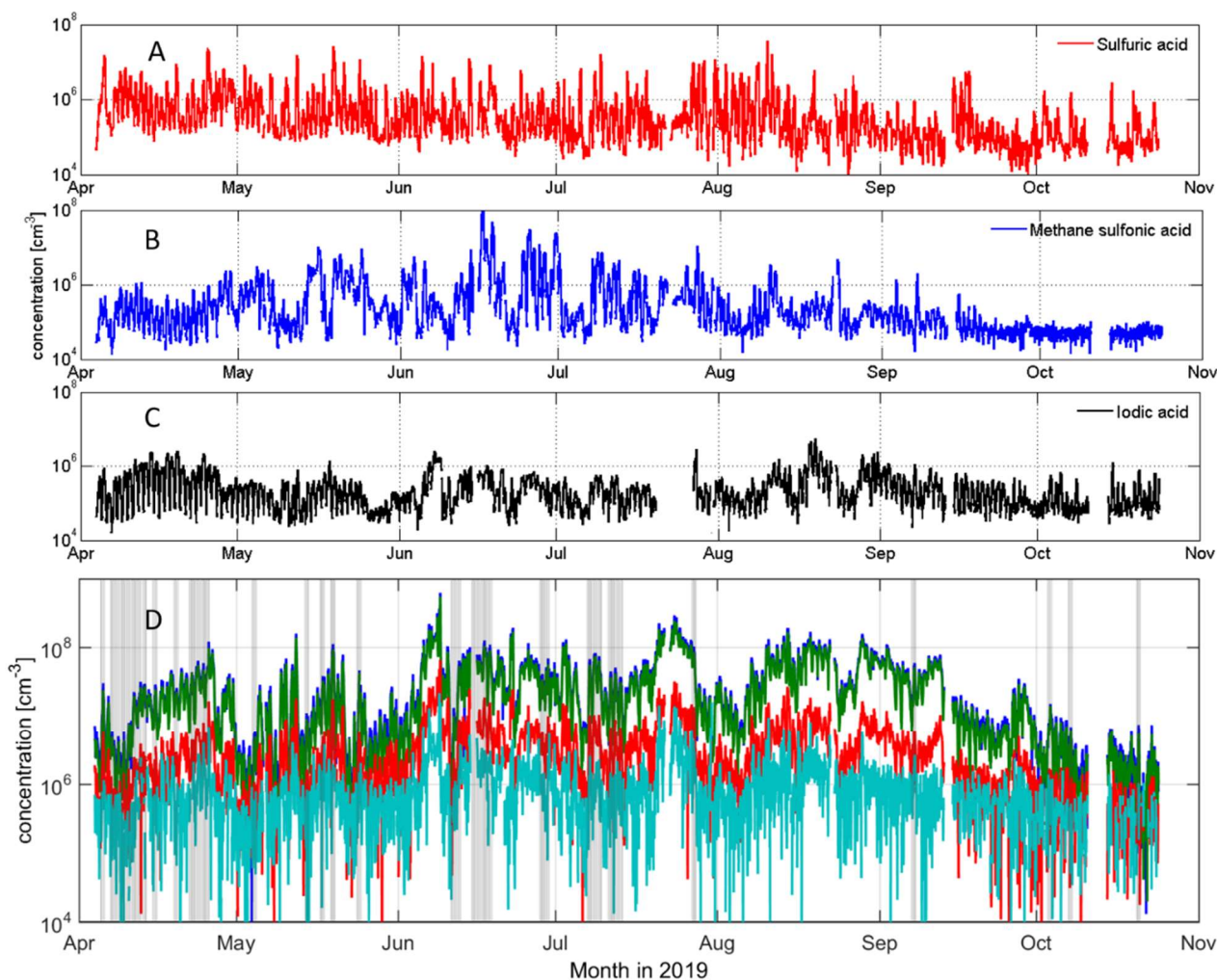
144 (Ehn et al., 2014; Sipilä et al., 2016), so the calibration factor for them should be similar, but please note, that  
145 the concentration of other compounds than SA can be highly uncertain due to different ionizing efficiencies,  
146 sensitivities and other unknown uncertainties. If MSA, IA or HOMs do not ionize at the kinetic limit these  
147 concentrations could be underestimated and thus, the concentrations reported in here should be taken as low  
148 limit values. The sulfuric acid, iodic acid and MSA data presented in this study are all results of high-resolution  
149 peak fitting of the CI-APi-TOF, in order to avoid inaccurate identification of compounds and to separate  
150 overlapping peaks. The HOM data is a sum of mass-to-charge ratios from 300 to 400 Th, representing the  
151 monomer HOM range ( $C_{10}$  compound range), 401 to 500 Th for the slightly larger HOMs ( $C_{15}$  compound  
152 range) and 501 to 600 Th for the dimer species ( $C_{20}$  compound range). We also give the sum of these all (from  
153 300 to 600 Th). The goal of this article is not to specify different HOM compounds or to study NPF in  
154 mechanistic details but to give an overview of general seasonal trends and variations of these selected species.  
155 Note that since this is a sum of all peaks in the selected mass range, we cannot assure that all the compounds  
156 included are HOMs. However, the investigation in laboratory conditions show that the nitrate-CI-APi-TOF is  
157 highly selective and sensitive towards HOMs with  $O > 5$  (Riva et al., 2019) and with hydroperoxide (-OOH)  
158 functionalities (Hytinen et al., 2015). All data obtained from the CI-APi-TOF we analyzed using tofTools  
159 program described in (Junninen et al., 2010) and averaged over an hour. The original data time resolution is 5  
160 sec. The uncertainty range of the measured concentrations reported in this study is estimated to be  
161  $-50\%/+100\%$  and the limit of detection, LOD  $4 \cdot 10^4$  molecules  $\text{cm}^{-3}$  (Jokinen et al., 2012).

162 To classify NPF events recorded during the measurement period, we used the data measured by a Differential  
163 Mobility Particle Sizer (DMPS). Condensation sink was also calculated using the DMPS data. The DMPS  
164 instrument and earlier statistics of NPF events in Värriö has been documented by (Dal Maso et al., 2007; Vana  
165 et al., 2016; Vehkamäki et al., 2004). The NPF events were classified according to (Maso et al., 2005). Total  
166 aerosol particle number concentration was measured with a Condensation Particle Counter (CPC, TSI 3776)  
167 in the size range of 3 – 800 nm. Air ion size distributions were measured with the Neutral cluster and Air Ion  
168 Spectrometer, NAIS (Kulmala et al., 2007; Manninen et al., 2016; Mirme and Mirme, 2013) that measures  
169 negative and positive ions in the size range of 0.8 – 42 nm in mobility diameter and total particle size  
170 distribution between  $\sim 2$  and 42 nm. All meteorological parameters, trace gas concentrations and aerosol data  
171 were downloaded directly from smartSMEAR open access database (<https://smear.avaa.csc.fi/>) and all mass  
172 spectrometric data are available on request.

### 173 3. Results and discussion:

#### 174 3.1. Overview of the whole measurement period:

175 You can see a time series of the most common aerosol precursor compounds; sulfuric acid, methane sulfonic  
176 acid, iodic acid and sums of different HOM groups in Figure 1. This figure depicts the whole measurement  
177 period from April 4 to October 27 in 2019. Overall, we succeeded to measure the whole 7 month period almost  
178 uninterrupted. Only a few short power cuts stopped our measurements during this time. Iodic acid data is  
179 missing from late July since its peak could not be separated well enough from overlapping peaks in the spectra  
180 during this time. This was due to poor resolution (low signal of  $\text{IO}_3^-$  close to another peak) that makes peak  
181 integration to give negative, unreal values and we thus decided to flag them out. After late October, the  
182 instrument malfunctioned and stopped our measurements. In this particular article, we present data from spring  
183 (Apr-May), summer (Jun-Jul-Aug) and autumn (Sep-Oct) 2019. More about the SMEAR I winter observations  
184 can be read in Sipilä et al., 2021 where they report observations of polar night pollution events from Värriö after  
185 the CI-APi-TOF was fixed.



186

187 **Figure 1.** Overview of sulfuric (A), methane sulfonic (B) and iodic acid (C), as well as HOM (D)  
 188 concentrations at SMEAR I in April to October 2019. NPF days are depicted in grey shading in panel D. All  
 189 data in panels A-C are resulting from high-resolution peak fitting. HOM data are sums of certain mass ranges;  
 190 from 300 to 400 Th in green, representing C10 or HOM monomer compounds, from 401 to 500 Th in red,  
 191 representing C15 compound and from 501 to 600 Th on light blue, representing C20 or HOM dimer  
 192 compounds. The sum of HOM (darker blue) is a sum of the aforementioned mass ranges. The sum of HOMs  
 193 is approximately one order of magnitude higher than SA, MSA or IA concentrations during this measurement  
 194 period.

195 In Figure 2 we show some of the most interesting environmental and meteorological parameters that influence  
 196 the atmospheric gas composition during the measurements period; temperature, global radiation and snow  
 197 depth, ozone, NO<sub>x</sub> and SO<sub>2</sub> mixing ratios. There are some special features in year 2019; the summer had two  
 198 heat waves, when the air temperature rose up to 29.2 °C in early June and to almost the same values in late  
 199 July. These episodes are getting more common in Lapland due to climate change. These warmer conditions  
 200 will probably change the emissions of trace gases including the composition and abundance of aerosol  
 201 precursors in the future Arctic environment (Schmale et al., 2021). However, heath wave conditions are likely  
 202 not favorable conditions to NPF since condensation of low-volatility gases is favored in colder temperatures  
 203 (via the vapor pressure decrease due to lower temperatures), but they may affect the oxidation chemistry of  
 204 VOCs by promoting dimer formation.

205 From Figure 2, we also see that the snow covered period ended in 2019 in late May and snow started to  
 206 accumulate again in mid-October. Solar radiation (Figure 2A) is intense in Värriö during springtime and gives

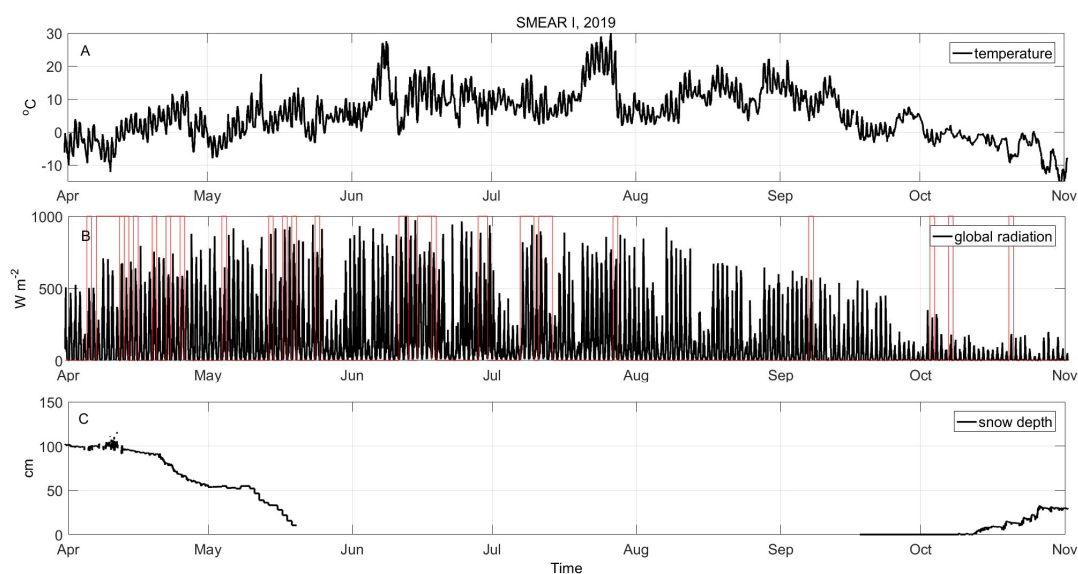


207 Väriö favorable photo-oxidizing conditions, effectively removing air pollutants and trace gases from the  
208 atmosphere. Photochemical activity in presence of NO<sub>x</sub> (Figure 2E), produces ozone in springtime and this is  
209 visible in very high ozone mixing ratios at the site (Figure 2D). Median ozone mixing ratios were around 55  
210 ppbv in April and decreased to ~30 ppbv in the late summer and autumn. The spring ozone mixing ratio in  
211 2019 was significantly higher than the previous reports from the years 1992 to 2001, when monthly mean  
212 values of ozone varied between 25 – 40 ppbv (Ruuskanen et al., 2003).

213 The springtime diurnal solar cycle is clearly visible with all studied compounds. All measured aerosol  
214 precursor compounds are abundant even during the period when snow covers the ground in the spring. The  
215 HOM concentrations follow the increasing solar radiation and rising temperature. MSA has a stronger diurnal  
216 cycle before the snow melt than after it. This may be due to rain and cloudy conditions that are more common  
217 in the summer. Sulfuric acid and iodic acid do not have such strong seasonal variation than HOMs and MSA.  
218 The aerosol precursor concentrations are discussed in more detail in the following sections.

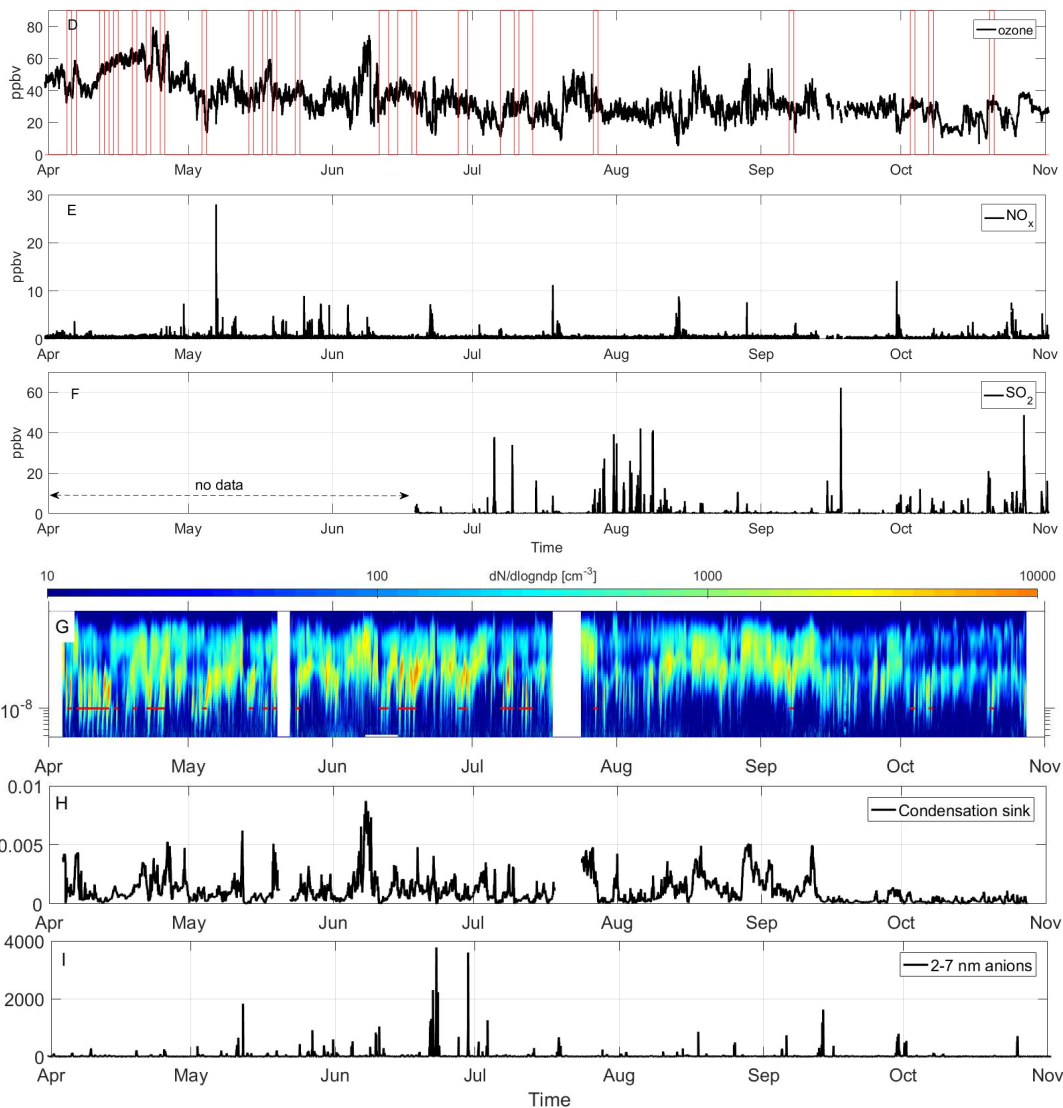
### 219 3.2. Seasonal and monthly variation of SA, MSA, iodic acid and HOM concentrations

220 We present the diurnal variation of aerosol precursors; sulfuric acid, methane sulfonic acid, iodic acid and  
221 highly oxygenated molecules, concentrations separately for different seasons accompanied with solar radiation  
222 and total aerosol number concentrations in Figure 3. Strong seasonality is most evident in sulfuric acid and  
223 HOM concentrations. SA is at its highest in the spring, decreasing toward summer and autumn while HOMs  
224 reach their maximum in the summer. We detect an increase in total aerosol number concentration on the spring  
225 evenings that is likely due to more frequent NPF events taking place at SMEAR I. The increase in HOMs in  
226 the summer at SMEAR I is linked to the increased emissions of VOCs from vegetation that oxidize into HOMs  
227 via ozonolysis (Ehn et al., 2014) and OH-radical reactions (Berndt et al., 2016; Jokinen et al., 2014, 2017;  
228 Wang et al., 2018). The overall lowest aerosol precursor concentrations and aerosol number concentration we  
229 detect during autumn (winter data was missing from this study, see Sipilä et al. 2021, for winter time  
230 observations made promptly after the period reported here). MSA shows very similar concentrations during  
231 spring and summer, and drops down to the limit of detection level for autumn. Iodic acid acts very differently  
232 than the other compounds. We observe iodic acid to have a similar level of concentration throughout the  
233 measurement period and seems that the concentration reaches a steady state during daylight hours. This  
234 daytime maximum stays at the same level about 5 hours longer during spring than in the autumn. The day  
235 length getting shorter towards the autumn explains this behavior. The maximum hourly median concentrations  
236 for the measured compounds are  $\sim 2 \cdot 10^6 \text{ cm}^{-3}$  for SA (spring),  $\sim 5 \cdot 10^5 \text{ cm}^{-3}$  for MSA (summer),  $\sim 3 \cdot 10^5 \text{ cm}^{-3}$   
237 for iodic acid (all seasons) and  $\sim 5 \cdot 10^7 \text{ cm}^{-3}$  for the sum of HOMs (summer, mass range from 300 to 600  
238 Th).



239

240



241

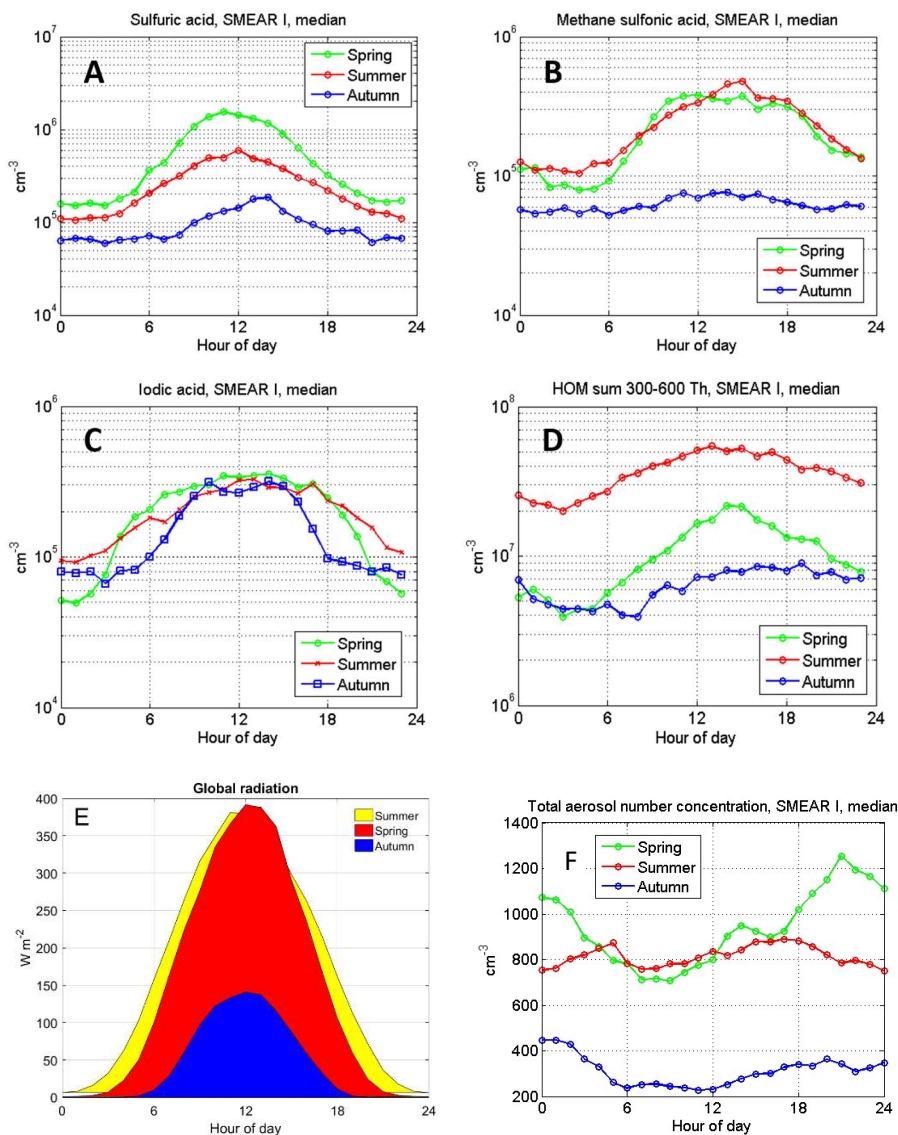
242

243 **Figure 2:** Observations of temperature (A), global radiation (B), snow depth (C), ozone (D), NO<sub>x</sub> (E) and SO<sub>2</sub>  
 244 (F) mixing ratios, number size distribution (G), condensation sink (H) and concentration of 2-7 nm anions (I)  
 245 at SMEAR I during the measurement period. SO<sub>2</sub> data is missing until mid-June due to instrumental  
 246 malfunction. NPF event times are depicted in red in subplots (B), (D) and (G).

247 We can compare these numbers to SMEAR II long-term (5-year median concentration) observations, where the  
 248 median peak SA concentrations are  $\sim 1.5 \cdot 10^6 \text{ cm}^{-3}$ ,  $\sim 1 \cdot 10^6 \text{ cm}^{-3}$  and  $\sim 3 \cdot 10^5 \text{ cm}^{-3}$  for spring, summer and  
 249 autumn, respectively (Sulo et al., 2021). These measured concentrations are very similar to SMEAR I  
 250 observations except a slightly higher summer and autumn SA concentration at SMEAR II. However, it should  
 251 be noted that the springtime measurements from SMEAR I do not include March data, which makes the  
 252 springtime comparison somewhat uncertain. However, as reported by Sipilä et al., 2021 the March data from  
 253 the following year seems very similar concentration levels what we report in here for spring (max.  $\sim 2 \cdot 10^6 \text{ cm}^{-3}$   
 254 and daily averages peak around  $0.5 \cdot 10^6 \text{ cm}^{-3}$ ). We expect that the SA concentrations are only marginally  
 255 affected by the lack of March data, but that the level of HOMs or MSA or IA could be affected more due to  
 256 very different meteorological conditions between the stations in springtime (SMEAR II is  $\sim 700 \text{ km}$  more South  
 257 than SMEAR I). There is also a difference in the timing of the peak SA concentration in the summer. At  
 258 SMEAR I the peak concentration is reached at noon and at SMEAR II it can be found some hours earlier,  
 259 already around eight o'clock in the morning (Sulo et al., 2021). In the case of HOMs, we cannot compare the  
 260 concentrations directly to Sulo et al. (2021) as they calculated the sum of HOMs differently, only taking into

261 account the most abundant signals and separating nitrate and non-nitrate HOMs. However, we take the liberty  
 262 to compare diurnal and seasonal variations. Both at SMEAR I and II, observations show the highest HOM  
 263 concentrations during summer, while the autumn concentrations are one order of magnitude lower. The  
 264 comparison between these sites reveals a different diurnal variation of HOMs. At SMEAR I, the HOMs have  
 265 a maximum around noon, spanning to the afternoon (Figure 3). At SMEAR II, HOMs have two maxima, one  
 266 at noon and another one in the early evening. From these, the latter is connected to non-nitrate monomer and  
 267 dimer HOMs and nitrate dimer HOMs. At SMEAR I the lack of an evening maximum could indicate that  
 268 HOM dimer formation is less dominant at SMEAR I compared to SMEAR II due to lower air temperatures,  
 269 or due to the different diurnal cycle of oxidants due to longer hours of solar radiation North of the Arctic Circle.

270



271

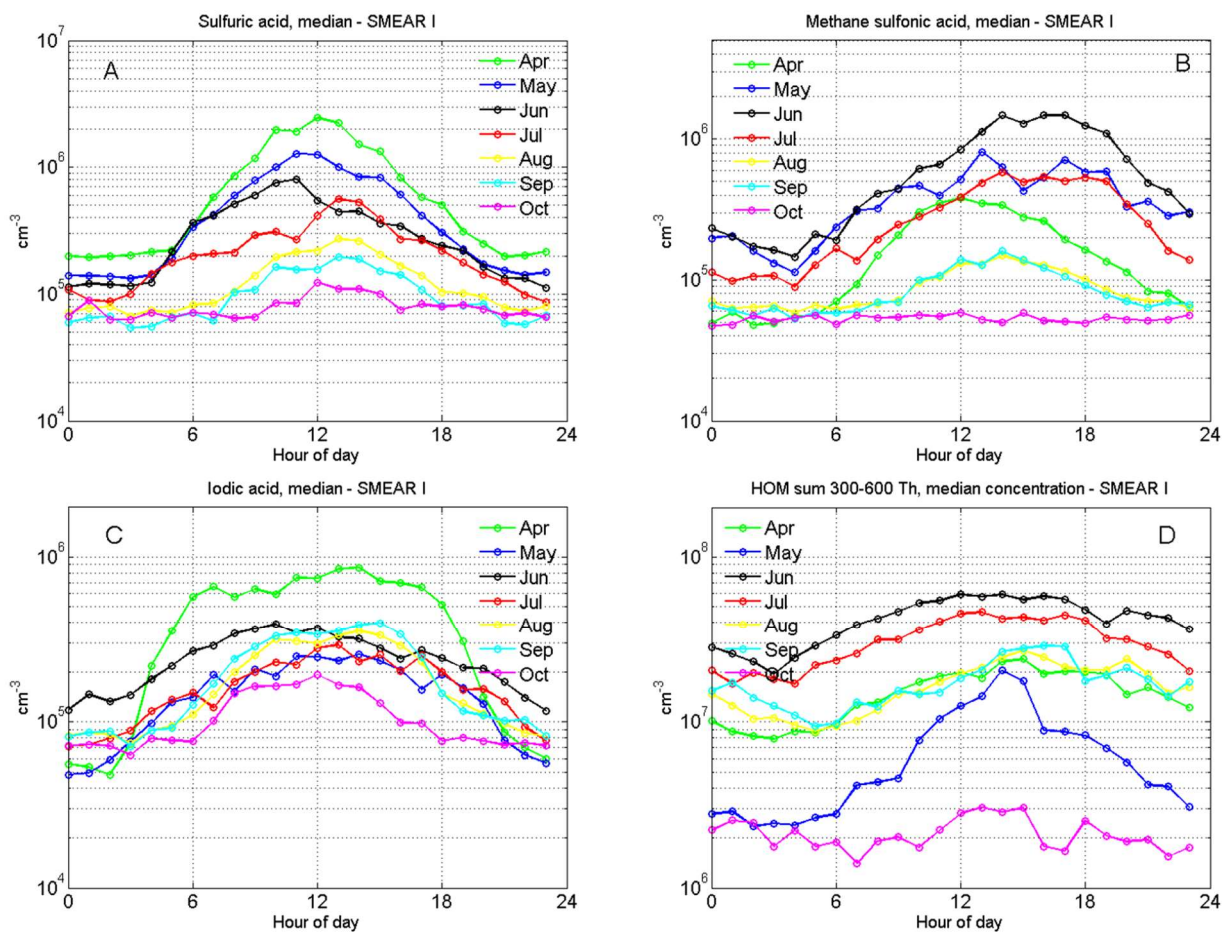
272

273 **Figure 3.** Diurnal variation of aerosol precursor gas median concentrations in different seasons: A) sulfuric  
 274 acid, B) methane sulfonic acid, C) iodic acid and D) the sum of HOMs in the 300 to 600 Th mass range. Panel  
 275 E) depicts the seasonal variation of global radiation and F) the total aerosol number concentration  $N_{tot}$ . The  
 276 small (false) offset (6-7  $W m^{-2}$ ) in summer data is due to 24 h sunlight hours at Värriö.

277 When analyzing the monthly aerosol precursor profiles in Figure 4, we observe that the springtime atmosphere  
 278 is abundant in SA and iodic acid that have the highest median concentrations in April. MSA and HOMs  
 279 concentrations peak in June. The MSA behavior is likely connected to the algae blooms in the Arctic Ocean  
 280 that peak around midsummer. The marine emissions of DMS oxidize in the atmosphere to sulfur dioxide,



281 sulfuric acid and to MSA (e.g. Park et al., 2018). However, sulfuric acid has more sources, since SO<sub>2</sub> has also  
 282 anthropogenic sources. At SMEAR I we cannot distinguish these sources precisely (more discussion about this  
 283 in section 3.3.). It is notable that the peak concentration of MSA is earlier in the day in April, around 12 o'clock  
 284 noon, than it is later in the year when the peak concentration is reached in the late afternoon (from 13:00 to  
 285 18:00 o'clock). There are no previous MSA concentration reports from the SMEAR stations but some gas  
 286 phase MSA results from Antarctica show maximum of  $1 \cdot 10^5 \text{ cm}^{-3}$  to  $1 \cdot 10^7 \text{ cm}^{-3}$  concentrations (Jokinen et  
 287 al., 2018; Mauldin et al., 2010, 2004). In the Arctic, around half a year measurement series from Villum in  
 288 Greenland show MSA concentrations  $<10^6 \text{ cm}^{-3}$  (Mar – Sep) and from  $10^5 \text{ cm}^{-3}$  to  $10^7 \text{ cm}^{-3}$  with the highest  
 289 concentrations in June in Ny-Ålesund (Beck et al., 2021). Our measurements from the SMEAR I fall in  
 290 between these extremes.



291

292 **Figure 4.** Monthly median concentrations of A) sulfuric acid, B) methane sulfonic acid, C) iodic acid and d)  
 293 the sum of HOMs in the 300 to 600 Th mass range.

294 These are also the first reported results of iodic acid measurements from SMEAR I and they represent a  
 295 continental location, the White Sea coast being ~130 km South East and the Barents sea ~230 km to the North  
 296 East. Iodic acid, iodine and iodic oxoacid emissions are commonly connected to coastal or marine  
 297 environments (Baccarini et al., 2020; McFiggans et al., 2010; O'dowd et al., 2002; Sipilä et al., 2016; Yu et  
 298 al., 2019) due to the fact that the ocean surface is a major source of iodine (Carpenter et al., 2013). While it is  
 299 not precisely known how iodic acid forms in the gas phase, its formation requires oxidation of the initial  
 300 precursors (IO<sub>x</sub> species) by ozone and the last steps of its formation is potentially driven by reaction with OH  
 301 (Chameides and Davis, 1980).

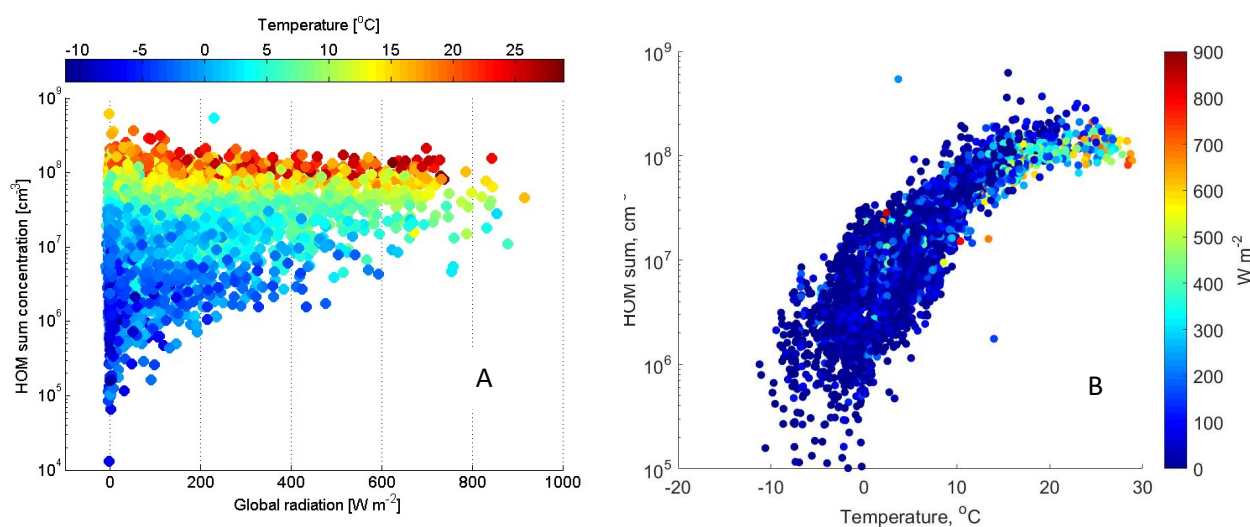
302 Compared to the other precursor compounds, iodic acid has the most stable concentration between seasons,  
 303 with a long increasing period in April during the snow-melting season. This is likely due to the simultaneously  
 304 increasing ozone mixing ratios (Figure 2D) and solar radiation. In contrast to measurements from the Arctic

305 Ocean (Baccarini et al., 2020), we did not observe a clear increase in iodic acid concentration in the autumn  
306 due to freezing. We find that September had only marginally higher concentrations compared to August or  
307 July (Figure 4). Winter measurements would be necessary to estimate the effect of freezing in the concentration  
308 of IA.

309 The source of iodic acid on a continental site like the SMEAR I is an interesting subject to speculate. The  
310 observed HIO<sub>3</sub> peak in April could indicate that there could be an influence from air masses exposed to Arctic  
311 marine environment, due to ocean surface acting as a major source of atmospheric iodine (Carpenter et al.,  
312 2013). The increasing temperature in the spring induce a higher activity of phytoplankton in the nearby Barents  
313 Sea and Norwegian Sea that remains ice free, even during the winter, and could result in the higher emission  
314 of precursors for iodic acid (Lai et al., 2011). Higher temperature would also result in more efficient advection,  
315 which would transport species faster from emission points to SMEAR I. The calculated back trajectories  
316 support the idea that iodine-rich air masses arrive from the West or northwest to SMEAR I (discussed in details  
317 in section 3.3. New Particle Formation events and Figure 10). This would be the hypothesis of the long-range  
318 transport for source of iodic acid in SMEAR I. On the contrary, the strong diurnal variation on iodic acid  
319 concentration seen as one order of magnitude difference between noon and midnight, suggests fast on-site  
320 chemistry, which is not consistent with long-range transport of iodic acid, but its precursor such as CH<sub>3</sub>I (Bell  
321 et al., 2002). Also, iodic acid life time against condensational loss is expected to be short with the condensation  
322 sink at the site (Figure 2H), in the range of ~15 minutes, this suggests that HIO<sub>3</sub> is formed close to or at the  
323 site of measurements. Land vegetation is a source of methyl iodide (CH<sub>3</sub>I) that could be the source of iodic  
324 acid at SMEAR I, at least during summer (Sive et al., 2007).

325 Most interestingly, we seem to have an emission source of iodine during all seasons. There are no reports on  
326 iodine emissions from continental snow, but we hypothesize that one possible source of iodine in SMEAR I  
327 during spring is the snowpack. This is possible due to the deposition of sea salts on snow particularly during  
328 dark periods that activate during the spring and are re-emitted to the atmosphere through heterogeneous  
329 photochemistry of iodide, and iodate ions (Raso et al., 2017; Spolaor et al., 2019). There are also possible  
330 forest emissions of iodinated organics, similar to New England growing season (Raso et al., 2017), that might  
331 be enhanced by higher temperature or high ozone concentrations. This type of emissions of iodinated gases,  
332 or their implications, have not been studied before but these observations might direct research into emission  
333 studies at SMEAR I, since our findings indicate that vegetation could be an emission source of iodine.

334 The sum of HOMs in SMEAR I reaches up to a median  $\sim 5 \cdot 10^7$  cm<sup>-3</sup> concentration in the summer. This is  
335 about one order of magnitude lower than the concentrations reported from the SMEAR II station in Hyytiälä  
336 (Yan et al., 2016) about 700 km south, where HOMs are at a maximum of  $\sim 6 \cdot 10^8$  cm<sup>-3</sup> during spring daytime.  
337 It is striking how well the concentration of HOMs follow the air temperature (Figure 5) but seem to level above  
338 circa 18°C. From the temperature dependency, we can speculate that most VOCs emitted by vegetation close  
339 to Värriö could be monoterpenes due to their strong temperature dependency. This is supported by emission  
340 rate measurements of VOCs showing that in northern Finland 60 to 85 % are accounted by  $\alpha$ - and  $\beta$ -pinene  
341 emissions (Tarvainen et al., 2004). However, sesquiterpene emissions from nearby wetlands could contribute  
342 to HOMs since their emissions are also temperature dependent and they are emitted by the boreal wetlands  
343 (Hellén et al., 2020; Seco et al., 2020). As HOMs are oxidation products of VOCs, it is evident that the HOM  
344 concentration will increase in SMEAR I in the future with the increasing VOC emissions, including isoprene,  
345 monoterpenes and sesquiterpenes, due to temperature rise (Ghirardo et al., 2020; Tiiva et al., 2008; Valolahti  
346 et al., 2015).



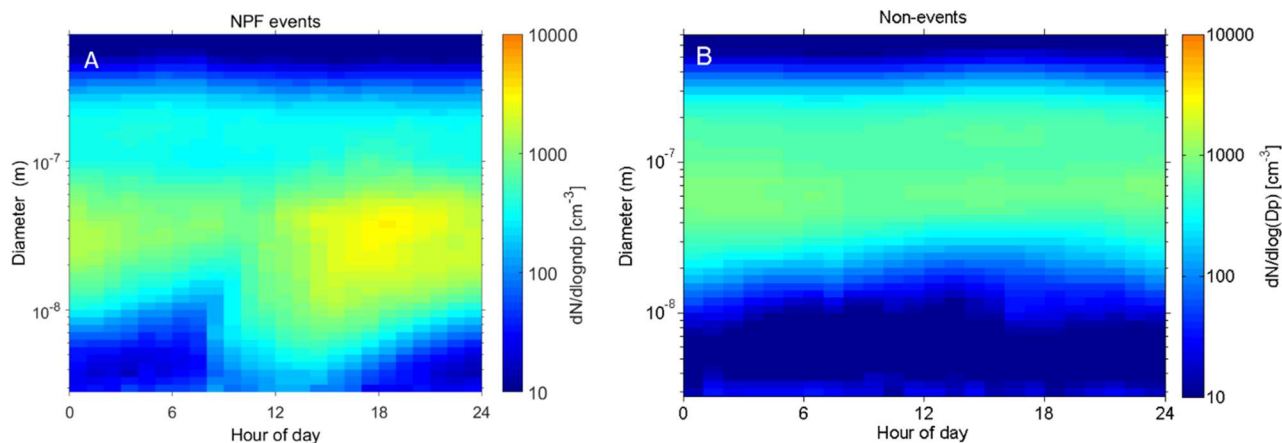
348 **Figure 5.** HOM concentration (cm<sup>-3</sup>) measured at SMEAR I (sum of mass range from 300 to 600 Th) as a  
 349 function of global radiation (W m<sup>-2</sup>) in panel A and as a function of temperature in panel B. The color bar  
 350 represents air temperature in °C (A) and global radiation (B). The plot includes all data measured from April  
 351 to October 2019.

### 352 3.3. New particle formation events;

353 During the measurement period from 4 April 2019 to 27 October 2019, we observed 36 regional NPF events  
 354 in total and our CI-API-TOF data covers 33 of these NPF days. During the same period, we observed 75 non-  
 355 event days without clear signs of particle formation (Maso et al., 2005). Rest of the days during our  
 356 measurement period were defined as undefined, bad data or partly bad data days and these were excluded from  
 357 our analysis. In this chapter, we focus on trace gases, meteorological parameters and detected aerosol precursor  
 358 gases during NPF days and compare them to non-event days.

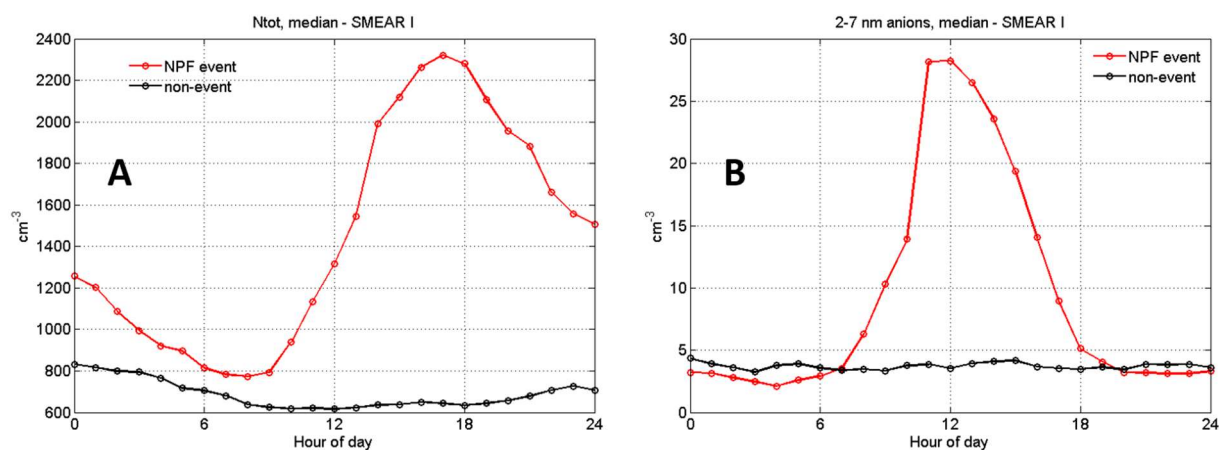
359 We plot NPF and non-event days median average number size distribution of aerosol particles (from 3 to 800  
 360 nm) in Figure 6, and the total number concentration and the 2-7 nm air ion concentrations in Figure 7. The  
 361 whole measurement period is represented already in Figure 2. In figure 6, in the case of NPF event days we  
 362 see a distinct “banana” plot, where small < 10 nm, particles are forming and growing with time. The DMPS  
 363 data is plotted from 2.82 nm to 708 nm but note that the channels below ~5 nm have much larger uncertainties  
 364 than those above. The median event start time is located around noon and the growth of particles continues  
 365 steadily until midnight. However, when looking at individual days, there is a large variation in the start-times  
 366 of the particle formation, some events start early in the morning or even in the night, while some start in late  
 367 afternoon. Non-event days show very few particles in the < 10 nm size bins.

368 The total number of particles measured at the site during NPF events rises up to ~2400 cm<sup>-3</sup> reaching the  
 369 maximum concentration at ~17 o’clock in the evening. This shows that NPF is an important source of aerosol  
 370 particles in Värriö as previously reported (Vehkamäki et al., 2004). Non-event days have clearly lower particle  
 371 concentrations throughout the day, staying lower than 1000 cm<sup>-3</sup> on average. The measured 2-7 nm anion  
 372 concentrations stay very low during non-event days. As intermediate ions form mainly during NPF, their  
 373 concentrations are used as indicator of NPF events in boreal environments (Leino et al., 2016). On NPF days,  
 374 we see a peak in the anion concentration at noon, the concentration being about six times higher than during  
 375 non-event days. This indicates that negative ions may play a role in SMEAR I particle formation events.



376

377 **Figure 6.** This figure depicts the median number size distribution during all observed NPF events ( $n = 33$ ) and  
 378 non-events ( $n = 75$ ) during our measurement period. The data is collected with a DMPS and size bins from  
 379 2.82 to 708 nm are plotted.

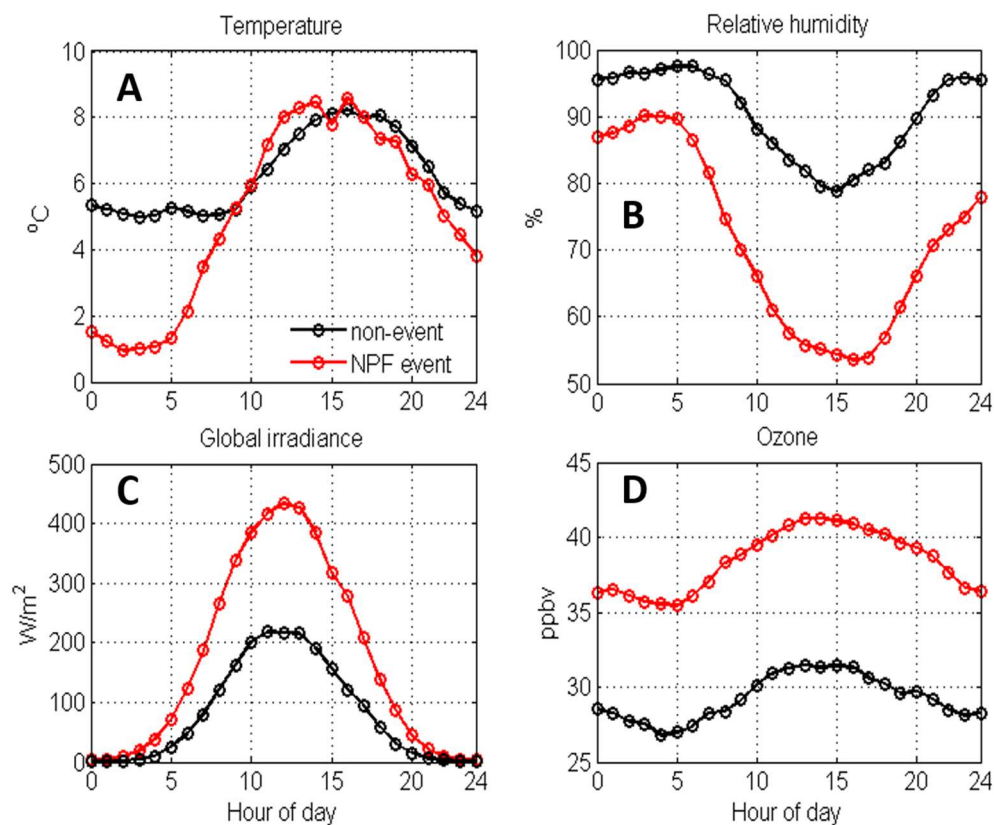


380

381 **Figure 7.** Median total particle concentration ( $N_{\text{tot}}$ ) in A) and 2-7 nm negative ion concentrations in B) at  
 382 SMEAR I during NPF event (red,  $n = 33$ ) and non-event days (black,  $n = 75$ ). The total particle number  
 383 concentration is recorded with a CPC and air ion concentrations with a NAIS.

384 Figure 8 shows the differences in temperature, relative humidity, global radiation and ozone mixing ratios  
 385 between NPF event days (in red) and non-event days (black). In Värriö, NPF events preferably happen in  
 386 relatively low temperatures ( $1 - 8$  °C) with a fast temperature rise in the early morning hours, lower and  
 387 decreasing RH, dropping from 90% to ~55 %, during the NPF days compared to non-event days. NPF days  
 388 have clearly higher global irradiance values ( $\sim 450$   $\text{m}^{-2}$  vs.  $\sim 200$   $\text{m}^{-2}$ ) and about 10 ppbv higher ozone  
 389 concentrations than non-event days. The meteorological conditions favor NPF are thus similar than at the  
 390 SMEAR II station in Hyytiälä, where sunny clear sky days with low RH and condensation sink along with  
 391 wind directions from the cleaner northerly sector are forecasting NPF events (Nieminen et al., 2014).



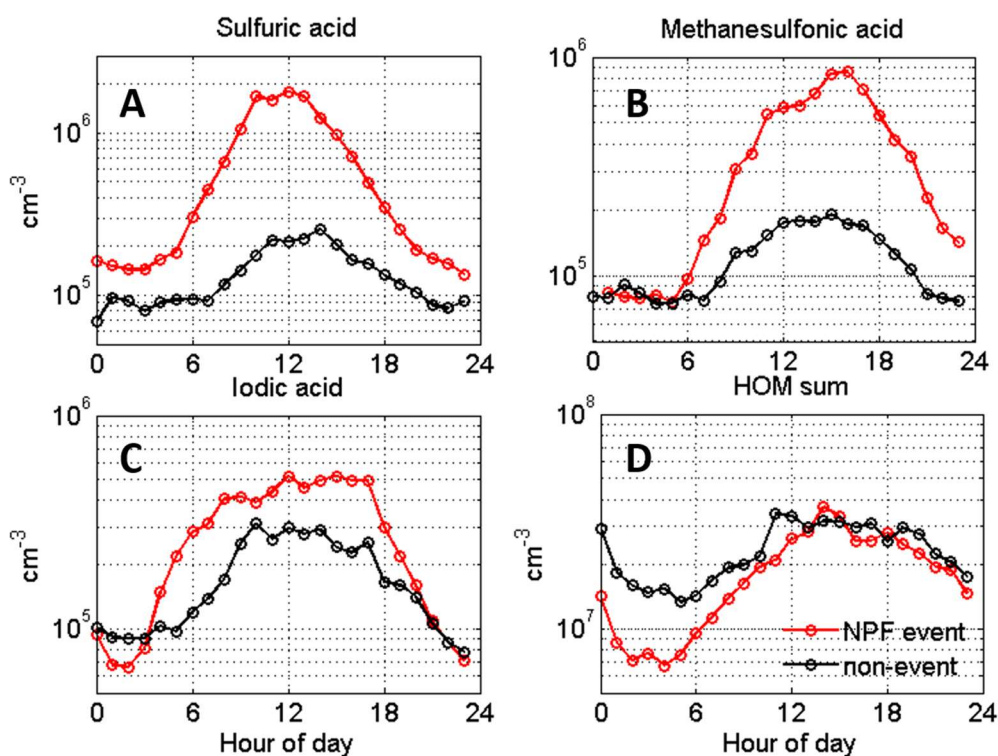


392

393 **Figure 8.** Average temperature (°C) in panel A), relative humidity (%) in B), global radiation ( $\text{W m}^{-2}$ ) in C)  
 394 and ozone concentration (ppbv) in D), all measured at SMEAR I during NPF event (red,  $n = 33$ ) and non-event  
 395 days (black,  $n = 75$ ).

396 Next, we show the concentrations of aerosol precursor compounds during NPF and non-event days in figure  
 397 9. The sulfuric acid concentrations closely follow the solar irradiation profile (Figure 8C). Similarly to the  
 398 results obtained from the high Arctic, Svalbard, also MSA is elevated during NPF events, especially during  
 399 summer, and could possibly contribute aerosol growth (Beck et al., 2021). We observe close to an order of  
 400 magnitude higher MSA concentration between the events and non-events days, highlighting the dominant role  
 401 of sulfur species to nucleation and growth in general at this site. In order to attribute the source of sulfur species  
 402 and IA during the event and non-event days we performed a cluster analysis using a geographical information  
 403 system (GIS) based software, Trajstat (Wang et al., 2009). The NCEP/NCAR reanalysis data was used as  
 404 meteorological input for the model (Kalnay et al., 1996). The simulations were performed at an arrival height  
 405 of 250 m. a.g.l. SMEAR I station is located approximately at similar height (390 m a.s.l), thus representing the  
 406 air masses arriving at the station even during strong temperature inversions (Sipilä et al., 2021).





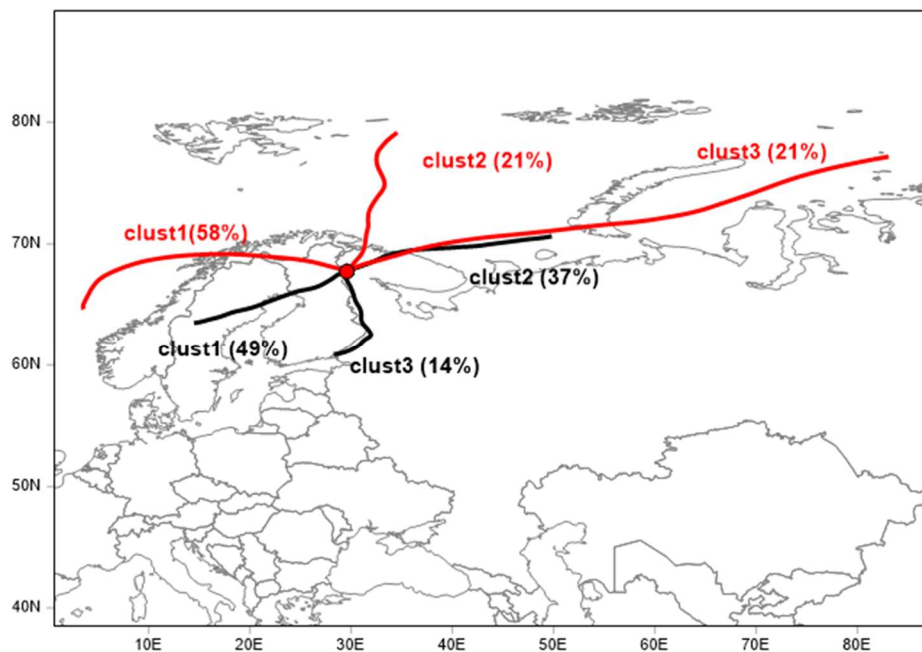
407

408 **Figure 9.** Aerosol precursor gases in SMEAR I during NPF (red,  $n = 33$ ) and non-event days (black,  $n = 75$ ).  
 409 The data is hourly median average.

410 Higher concentrations of aerosol precursors SA, MSA and IA are connected to the air masses that arrive to  
 411 SMEAR I from the Arctic Ocean (Figure 10). Cluster analysis of air mass back trajectories arriving to Värriö  
 412 during NPF days clearly shows, that most NPF events occur when the air mass was exposed to marine  
 413 environments within the last 72 hours. In our case, mainly the Norwegian Sea in the West (58 %) or the Barents  
 414 (21 %) and Kara Seas (21 %) in the Arctic Ocean. This seems relevant to our results since the marine  
 415 environment in the North is emitting large amounts of dimethyl sulfide (DMS), a precursor for SA and MSA  
 416 (Levasseur, 2013) and iodine species that further oxidize to IA (Baccarini et al., 2020; Sherwen et al., 2016).  
 417 A fraction of air masses that are connected to both NPF (21 %) and non-event days (37 %) are coming to  
 418 SMEAR I from the Kola peninsula that is connected to high  $\text{SO}_2$  emissions, higher particle number  
 419 concentrations and winter time NPF events (Sipilä et al., 2021). Most non-event air masses arrive to Värriö  
 420 from South-West (49 %) crossing northern Finland and Sweden.

421 In addition from Figure 9 we observe that we cannot rule out the contribution of iodic acid in NPF in SMEAR  
 422 I, but with the recorded concentration, it usually is not enough to initiate NPF (He et al., 2021). Although iodic  
 423 acid concentrations are slightly larger on NPF days than non-event days, the rise in concentration happens  
 424 already early in the morning, clearly before the average event start-time. The possible source of iodic acid was  
 425 discussed earlier in chapter 3.2 and we hypothesize that the source of iodine at SMEAR I could be both; i) the  
 426 long distance transport from the Arctic Ocean combined to ii) the local emissions from the snow pack and  
 427 vegetation. The hypothesis of vegetation emitted iodine species is supported by the minor difference between  
 428 NPF (mostly marine) and non-event day (mostly continental) concentrations. At SMEAR I, HOMs are the  
 429 only species that are at a (marginally) lower level during non-event than NPF days indicating that the total  
 430 HOM concentration does not determine when NPF events occur. However, this does not exclude the possible  
 431 participation of certain HOMs in NPF together with sulfur compounds (Lehtipalo et al., 2018) or at later stages  
 432 of the NPF process, especially during particle growth. However, pure biogenic nucleation involving ions and  
 433 HOMs (Kirkby et al., 2016) seems not to be a major NPF pathway in Värriö.

434 Our measurements do not unveil the detailed mechanism of nucleation or growth of particles. We lack  
435 measurements of ambient bases that are needed to stabilize sulfuric acid clusters in ambient conditions (e.g.  
436 Almeida et al., 2013; Jen et al., 2014; Kirkby et al., 2011; Kürten et al., 2014; Myllys et al., 2018). With the  
437 given observations comparing NPF days with non-event days it is likely that most regional NPF events require  
438 sulfuric acid, but the NPF process can involve other compounds as well, especially IA and MSA, which show  
439 higher concentrations on NPF days, very similarly that the results reported from Ny-Ålesund (Beck et al.,  
440 2021).



441

442 **Figure 10.** Trajectory cluster analysis of 72-hour back trajectories simulated at arrival height of 250 m a.g.l  
443 and the NCEP/NCAR reanalysis data used as meteorological input. Red = NPF event, black = non-NPF

#### 444 4. Conclusions:

445 We report ~7 months of nitrate-based CI-API-TOF measurements of sulfuric acid, methane sulfonic acid, iodic  
446 acid and highly oxygenated organic compounds from a remote sub-Arctic field station SMEAR I in Finland.  
447 The measurements aim to increase our understanding of the Arctic aerosol forming precursors and atmospheric  
448 chemistry in more details. The reason for measuring these compounds ~150 km north of the Arctic Circle is  
449 simple; the Arctic is warming twice the speed as the planet on average. Lapland is already facing environmental  
450 changes when e.g. woody plants disperse further north and influence the tundra ecosystem (Aakala et al., 2014;  
451 Kempainen et al., 2021). These changes will in turn affect the emissions of aerosol precursor gases, which  
452 may have feedback effects on to the climate (e.g. Kulmala et al., 2020; Paasonen et al., 2013).

453 The area surrounding SMEAR I station has snow cover for almost 8 months a year. Accumulating snow during  
454 the autumn is a good reservoir to e.g. halogens, similarly than in the high Arctic (and Arctic Ocean)  
455 environment. The snow pack also acts as a cover for biogenic emissions entering the atmosphere from the  
456 ground. Any changes in the temperature and snow cover in the sub-Arctic regions will effect on atmospheric  
457 chemistry and composition that are undeniably changing the way aerosol particles form and what their number  
458 concentration is in the region.

459 In this study, we report seasonal and monthly variations of SA, MSA, IA and HOM concentrations and find  
460 all these compounds abundant in springtime. SA has a peak concentration in the spring, decreasing for the rest  
461 of the seasons. We detect high concentrations of MSA and IA that are usually connected to marine and coastal  
462 environments, although Värriö is located ~130 km from the nearest coast of the White Sea. While MSA is

463 abundant in the spring, summer and decreases to limit of detection levels for autumn, IA continues at the same  
464 concentration throughout the seasons. It seems likely that these two compounds are connected to emissions  
465 from phytoplankton or the Arctic ice pack and arrive to SMEAR I by long transport routes. In the case of iodine  
466 acid, we suggest that the source of iodine emissions is a combination of transport and local emission from the  
467 continental snow pack and vegetation at the site. Further work is needed to confirm this hypothesis.

468 The most striking correlation we found in HOM concentrations and ambient air temperature. The vegetation  
469 at SMEAR I is the source of VOCs even in the snow covered spring season and these volatile gases are oxidized  
470 into HOMs with different reaction rates depending on the oxidant. In the case of such strong temperature  
471 controlled HOM concentrations, we conclude that HOMs in the mass range of 300 – 600 Th are most likely  
472 products of monoterpene oxidation.

473 We also studied the abundance of these aerosol precursors separately during NPF and non-event days. We  
474 observed that new particles at SMEAR I preferably form in relatively low temperatures (< 10°C), low relative  
475 humidity that decreases with rising temperature during the day (to a minimum of ~55%), ~10 ppbv higher  
476 ozone mixing ratio than during non-event days, high SA concentration in the morning and high MSA  
477 concentrations in the afternoon. Cluster analysis of air masses show that NPF usually happens in marine air  
478 masses travelling to the site from North West – West. All together, these are the first long term measurements  
479 of aerosol forming precursor from the sub-arctic region helping us to understand atmospheric chemical  
480 processes and aerosol formation in the rapidly changing Arctic.

#### 481 **Data availability:**

482 All meteorological parameters, trace gas concentrations and aerosol data we downloaded directly from  
483 smartSMEAR open access database (<https://smear.avaa.csc.fi/>). All mass spectrometric data are available on  
484 request from the corresponding author.

#### 485 **Author contribution:**

486 TJ, MS, TP and MK designed the experiments at SMEAR I and MS, NS, KN and TL carried them out. IY  
487 made the NPF event analysis and RT calculated the back trajectories. TJ and KL wrote the manuscript with  
488 contributions from all co-authors.

#### 489 **Competing interests:**

490 Markku Kulmala is editor of ACP. Tuukka Petäjä is editor of ACP.

#### 491 **Acknowledgements:**

492 We would like to thank the technical staff in Kumpula and Värriö, who keep the long-term measurements  
493 going and helped with data collection, instrument calibrations, logistics and in data quality control and  
494 assurance during the year. We acknowledge the important role our collaborators have in scientific discussion  
495 and a special thanks goes to Alfonso Saiz-Lopez for iodine acid related discussion that helped to draft this  
496 article. We thank the ACTRIS CiGas-UHEL unit for mass spectrometer calibration support and the tofTools  
497 team for data analysis software.

#### 498 **Financial support:**

499 The Academy of Finland via Center of Excellence in Atmospheric Sciences (project no. 272041) and European  
500 Research Council via ATM-GTP 266 (742206), GASPARCON (714621) and Flagship funding (grant no.  
501 337549) funded this work. We also received funding from the Academy of Finland (project no. 1235656,  
502 296628, 316114, 315203, 307537, 325647, 33397, 334792 and 334514) “Quantifying carbon sink,  
503 CarbonSink+ and their interaction with air quality” and Academy professorship (grant no. 302958). This work  
504 was further supported by the European Commission via via project iCUPE (Integrative and Comprehensive  
505 Understanding on Polar Environments, No 689443), the EMME-CARE project which received funding from  
506 the European Union's Horizon 2020 Research and Innovation Programme, under grant agreement no. 856612,

507 Regional Council of Lapland (Värrion tutkimusaseman huippututkimus hyödyntämään Itä-Lapin  
508 elinkeinoelämää, VÄRI, A74190) and Aatos Erkko Foundation.

509 **References:**

- 510 Aakala, T., Hari, P., Dengel, S., Newberry, S. L., Mizunuma, T. and Grace, J.: A prominent stepwise  
511 advance of the tree line in north-east Finland, *J. Ecol.*, 102(6), 1582–1591, doi:10.1111/1365-2745.12308,  
512 2014.
- 513 Ahonen, T., Aalto, P., Rannik, Ü., Kulmala, M., Nilsson, E. D., Palmroth, S., Ylitalo, H. and Hari, P.:  
514 Variations and vertical profiles of trace gas and aerosol concentrations and CO<sub>2</sub> exchange in eastern  
515 Lapland, *Atmos. Environ.*, 31(20), 3351–3362, doi:10.1016/S1352-2310(97)00151-9, 1997.
- 516 Almeida, J., Schobesberger, S., Kürten, A., Ortega, I. K., Kupiainen-Määttä, O., Praplan, A. P., Adamov, A.,  
517 Amorim, A., Bianchi, F., Breitenlechner, M., David, A., Dommen, J., Donahue, N. M., Downard, A., Dunne,  
518 E., Duplissy, J., Ehrhart, S., Flagan, R. C., Franchin, A., Guida, R., Hakala, J., Hansel, A., Heinritzi, M.,  
519 Henschel, H., Jokinen, T., Junninen, H., Kajos, M., Kangasluoma, J., Keskinen, H., Kupc, A., Kurtén, T.,  
520 Kvashin, A. N., Laaksonen, A., Lehtipalo, K., Leiminger, M., Leppä, J., Loukonen, V., Makhmutov, V.,  
521 Mathot, S., McGrath, M. J., Nieminen, T., Olenius, T., Onnela, A., Petäjä, T., Riccobono, F., Riipinen, I.,  
522 Rissanen, M., Rondo, L., Ruuskanen, T., Santos, F. D., Sarnela, N., Schallhart, S., Schnitzhofer, R., Seinfeld,  
523 J. H., Simon, M., Sipilä, M., Stozhkov, Y., Stratmann, F., Tomé, A., Tröstl, J., Tsagkogeorgas, G.,  
524 Vaattovaara, P., Viisanen, Y., Virtanen, A., Vrtala, A., Wagner, P. E., Weingartner, E., Wex, H.,  
525 Williamson, C., Wimmer, D., Ye, P., Yli-Juuti, T., Carslaw, K. S., Kulmala, M., Curtius, J., Baltensperger,  
526 U., Worsnop, D. R., Vehkamäki, H. and Kirkby, J.: Molecular understanding of sulphuric acid-amine  
527 particle nucleation in the atmosphere, *Nature*, 502(7471), 359–363, doi:10.1038/nature12663, 2013.
- 528 Baccarini, A., Karlsson, L., Dommen, J., Duplessis, P., Vüllers, J., Brooks, I. M., Saiz-Lopez, A., Salter, M.,  
529 Tjernström, M., Baltensperger, U., Zieger, P. and Schmale, J.: Frequent new particle formation over the high  
530 Arctic pack ice by enhanced iodine emissions, *Nat. Commun.*, 11(1), doi:10.1038/s41467-020-18551-0,  
531 2020.
- 532 Beck, L. J., Sarnela, N., Junninen, H., Hoppe, C. J. M. M., Garmash, O., Bianchi, F., Riva, M., Rose, C.,  
533 Peräkylä, O., Wimmer, D., Kausiala, O., Jokinen, T., Ahonen, L., Mikkilä, J., Hakala, J. J., He, X.-C. C.,  
534 Kontkanen, J., Wolf, K. K. E. E., Cappelletti, D., Mazzola, M., Traversi, R., Petroselli, C., Viola, A. P.,  
535 Vitale, V., Lange, R., Massling, A., Nøjgaard, J. K., Krejci, R., Karlsson, L., Zieger, P., Jang, S. S., Lee, K.,  
536 Vakkari, V., Lampilahti, J., Thakur, R. C., Leino, K., Kangasluoma, J., Duplissy, E.-M. M., Siivola, E.,  
537 Marbouti, M., Tham, Y. J., Saiz-Lopez, A., Petäjä, T., Ehn, M., Worsnop, D. R., Skov, H., Kulmala, M.,  
538 Kerminen, V.-M. M., Sipilä, M., Nøjgaard, J., Krejci, R., Karlsson, L., Zieger, P., Jang, S. S., Lee, K.,  
539 Vakkari, V., Lampilahti, J., Thakur, R. C., Leino, K., Kangasluoma, J., Duplissy, E.-M. M., Siivola, E.,  
540 Marbouti, M., Tham, Y. J., Saiz-Lopez, A., Petäjä, T., Ehn, M., Worsnop, D. R., Skov, H., Kulmala, M.,  
541 Kerminen, V.-M. M. and Sipilä, M.: Differing Mechanisms of New Particle Formation at Two Arctic Sites,  
542 *Geophys. Res. Lett.*, 48(4), e2020GL091334, doi:10.1029/2020GL091334, 2021.
- 543 Bell, N., Hsu, L., Jacob, D. J., Schultz, M. G., Blake, D. R., Butler, J. H., King, D. B., Lobert, J. M. and  
544 Maier-Reimer, E.: Methyl iodide: Atmospheric budget and use as a tracer of marine convection in global  
545 models, *J. Geophys. Res. Atmos.*, 107(D17), ACH 8-1, doi:10.1029/2001JD001151, 2002.
- 546 Berndt, T., Richters, S., Jokinen, T., Hyttinen, N., Kurtén, T., Otkjær, R. V., Kjaergaard, H. G., Stratmann,  
547 F., Herrmann, H., Sipilä, M., Kulmala, M. and Ehn, M.: Hydroxyl radical-induced formation of highly  
548 oxidized organic compounds, *Nat. Commun.*, 7, 13677, doi:10.1038/ncomms13677, 2016.
- 549 Bianchi, F., Garmash, O., He, X., Yan, C., Iyer, S., Rosendahl, I., Xu, Z., Rissanen, M. P., Riva, M., Taipale,  
550 R., Sarnela, N., Petäjä, T., Worsnop, D. R., Kulmala, M., Ehn, M. and Junninen, H.: The role of highly  
551 oxygenated molecules (HOMs) in determining the composition of ambient ions in the boreal forest, *Atmos.*  
552 *Chem. Phys.*, 17(22), 13819–13831, doi:10.5194/acp-17-13819-2017, 2017.
- 553 Bradshaw, C. J. A. and Warkentin, I. G.: Global estimates of boreal forest carbon stocks and flux, *Glob.*  
554 *Planet. Change*, 128, 24–30, doi:10.1016/j.gloplacha.2015.02.004, 2015.

- 555 Brandt, J. P., Flannigan, M. D., Maynard, D. G., Thompson, I. D. and Volney, W. J. A.: An introduction to  
556 Canada's boreal zone: Ecosystem processes, health, sustainability, and environmental issues1, *Environ. Rev.*,  
557 21(4), 207–226, doi:10.1139/er-2013-0040, 2013.
- 558 Carpenter, L. J., MacDonald, S. M., Shaw, M. D., Kumar, R., Saunders, R. W., Parthipan, R., Wilson, J. and  
559 Plane, J. M. C.: Atmospheric iodine levels influenced by sea surface emissions of inorganic iodine, *Nat.*  
560 *Geosci.*, 6(2), 108–111, doi:10.1038/ngeo1687, 2013.
- 561 Chameides, W. L. and Davis, D. D.: Iodine: Its possible role in tropospheric photochemistry, *J. Geophys.*  
562 *Res. Ocean.*, 85(C12), 7383–7398, doi:10.1029/JC085IC12P07383, 1980.
- 563 Charlson, R. J., Lovelock, J. E., Andreae, M. O. and Warren, S. G.: Oceanic phytoplankton, atmospheric  
564 sulphur, cloud albedo and climate, *Nature*, 326(6114), 655–661, doi:10.1038/326655a0, 1987.
- 565 Dal Maso, M., Sogacheva, L., Aalto, P. P., Riipinen, I., Komppula, M., Tunved, P., Korhonen, L., Suur-Uski,  
566 V., Hirsikko, A., Kurtén, T., Kerminen, V.-M. M., Lihavainen, H., Viisanen, Y. Y., Hansson, H.-C. C.,  
567 Kulmala, M., Maso, M. D., Sogacheva, L., Aalto, P. P., Riipinen, I., Komppula, M., Tunved, P., Korhonen,  
568 L., Suur-Uski, V., Hirsikko, A., Kurtén, T., Kerminen, V.-M. M., Lihavainen, H., Viisanen, Y. Y., Hansson,  
569 H.-C. C., Kulmala, M., Dal Maso, M., Sogacheva, L., Aalto, P. P., Riipinen, I., Komppula, M., Tunved, P.,  
570 Korhonen, L., Suur-Uski, V., Hirsikko, A., Kurtén, T., Kerminen, V.-M. M., Lihavainen, H., Viisanen, Y.  
571 Y., Hansson, H.-C. C., Kulmala, M.: Aerosol size distribution measurements at four Nordic field stations:  
572 Identification, analysis and trajectory analysis of new particle formation bursts, *Tellus, Ser. B Chem. Phys.*  
573 *Meteorol.*, 59(3), 350–361, doi:10.1111/j.1600-0889.2007.00267.x, 2007.
- 574 Dall'Osto, M., Geels, C., Beddows, D. C. S., Boertmann, D., Lange, R., Nøjgaard, J. K., Harrison, R. M.,  
575 Simo, R., Skov, H. and Massling, A.: Regions of open water and melting sea ice drive new particle formation  
576 in North East Greenland., *Sci. Rep.*, 8(1), 6109, doi:10.1038/s41598-018-24426-8, 2018.
- 577 Ehn, M., Thornton, J. A., Kleist, E., Sipilä, M., Junninen, H., Pullinen, I., Springer, M., Rubach, F.,  
578 Tillmann, R., Lee, B., Lopez-Hilfiker, F., Andres, S., Acir, I.-H. H., Rissanen, M., Jokinen, T.,  
579 Schobesberger, S., Kangasluoma, J., Kontkanen, J., Nieminen, T., Kurtén, T., Nielsen, L. B., Jørgensen, S.,  
580 Kjaergaard, H. G., Canagaratna, M., Maso, M. D., Berndt, T., Petäjä, T., Wahner, A., Kerminen, V.-M. M.,  
581 Kulmala, M., Worsnop, D. R., Wildt, J. and Mentel, T. F.: A large source of low-volatility secondary organic  
582 aerosol, *Nature*, 506(7489), 476–479, doi:10.1038/nature13032, 2014.
- 583 Ghirardo, A., Lindstein, F., Koch, K., Buegger, F., Schloter, M., Albert, A., Michelsen, A., Winkler, J. B.,  
584 Schnitzler, J.-P. and Rinnan, R.: Origin of volatile organic compound emissions from subarctic tundra under  
585 global warming, *Glob. Chang. Biol.*, 26(3), 1908–1925, doi:10.1111/GCB.14935, 2020.
- 586 Hari, P., Aalto, P., Hämeri, K., Kulmala, M., Lahti, T., Luoma, S., Palva, L., Pohja, T., Pulliainen, E.,  
587 Siivola, E. and Vesala, T.: Air pollution in eastern Lapland: challenge for an environmental measurement  
588 station, *Silva Fenn.*, 28(1), 29–39, doi:10.14214/SF.A9160, 1994.
- 589 He, X.-C., Tham, Y. J., Dada, L., Wang, M., Finkenzeller, H., Stolzenburg, D., Iyer, S., Simon, M., Kürten,  
590 A., Shen, J., Rörup, B., Rissanen, M., Schobesberger, S., Baalbaki, R., Wang, D. S., Koenig, T. K., Jokinen,  
591 T., Sarnela, N., Beck, L. J., Almeida, J., Amanatidis, S., Amorim, A., Ataei, F., Baccarini, A., Bertozzi, B.,  
592 Bianchi, F., Brilke, S., Caudillo, L., Chen, D., Chiu, R., Chu, B., Dias, A., Ding, A., Dommen, J., Duplissy,  
593 J., Haddad, I. El, Carracedo, L. G., Granzin, M., Hansel, A., Heinritzi, M., Hofbauer, V., Junninen, H.,  
594 Kangasluoma, J., Kempainen, D., Kim, C., Kong, W., Krechmer, J. E., Kvashin, A., Laitinen, T.,  
595 Lamkaddam, H., Lee, C. P., Lehtipalo, K., Leiminger, M., Li, Z., Makhmutov, V., Manninen, H. E., Marie,  
596 G., Marten, R., Mathot, S., Mauldin, R. L., Mentler, B., Möhler, O., Müller, T., Nie, W., Onnela, A., Petäjä,  
597 T., Pfeifer, J., Philippov, M., Ranjithkumar, A., Saiz-Lopez, A., Salma, I., Scholz, W., Schuchmann, S.,  
598 Schulze, B., Steiner, G., Stozhkov, Y., Tauber, C., Tomé, A., Thakur, R. C., Väisänen, O., Vazquez-Pufleau,  
599 M., Wagner, A. C., Wang, Y., Weber, S. K., Winkler, P. M., Wu, Y., Xiao, M., Yan, C., Ye, Q., Ylisirniö,  
600 A., Zauner-Wieczorek, M., Zha, Q., Zhou, P., Flagan, R. C., Curtius, J., Baltensperger, U., Kulmala, M.,  
601 Kerminen, V.-M., Kurtén, T., et al.: Role of iodine oxoacids in atmospheric aerosol nucleation, *Science* (80-  
602 ), 371(6529), 589–595, doi:10.1126/SCIENCE.ABE0298, 2021.
- 603 Hellén, H., Schallhart, S., Praplan, A., Tykkä, T., Aurela, M., Lohila, A. and Hakola, H.: Terpenoid



604 measurements at a Northern wetland revealed a strong source of sesquiterpenes, *Atmos. Chem. Phys.*  
605 *Discuss.*, 1–20, doi:10.5194/ACP-2019-1154, 2020.

606 Hyttinen, N., Kupiainen-Määttä, O., Rissanen, M. P., Muuronen, M., Ehn, M. and Kurtén, T.: Modeling the  
607 Charging of Highly Oxidized Cyclohexene Ozonolysis Products Using Nitrate-Based Chemical Ionization, *J.*  
608 *Phys. Chem. A*, 119(24), 6339–6345, 2015.

609 IPCC, F. assessment report: Fifth Assessment Report - Climate Change 2013, IPCC, Fifth Assess. Rep. -  
610 *Clim. Chang.* [online] Available from: <http://www.ipcc.ch/report/ar5/wg1/>, 2013.

611 Jen, C. N., McMurry, P. H. and Hanson, D. R.: Stabilization of sulfuric acid dimers by ammonia,  
612 methylamine, dimethylamine, and trimethylamine, *J. Geophys. Res. Atmos.*, 119(12), 7502–7514,  
613 doi:10.1002/2014JD021592, 2014.

614 Jokinen, T., Sipilä, M., Junninen, H., Ehn, M., Lönn, G., Hakala, J., Petäjä, T., Mauldin, R. L., Kulmala, M.  
615 and Worsnop, D. R.: Atmospheric sulphuric acid and neutral cluster measurements using CI-APi-TOF,  
616 *Atmos. Chem. Phys.*, 12(9), 4117–4125, doi:10.5194/acp-12-4117-2012, 2012.

617 Jokinen, T., Sipilä, M., Richters, S., Kerminen, V.-M. M., Paasonen, P., Stratmann, F., Worsnop, D.,  
618 Kulmala, M., Ehn, M., Herrmann, H. and Berndt, T.: Rapid autoxidation forms highly oxidized RO<sub>2</sub> radicals  
619 in the atmosphere, *Angew. Chemie Int. Ed.*, 53(52), 14596–14600, doi:10.1002/anie.201408566, 2014.

620 Jokinen, T., Kontkanen, J., Lehtipalo, K., Manninen, H. E., Aalto, J., Porcar-Castell, A., Garmash, O.,  
621 Nieminen, T., Ehn, M., Kangasluoma, J., Junninen, H., Levula, J., Duplissy, J., Ahonen, L. R., Rantala, P.,  
622 Heikkinen, L., Yan, C., Sipilä, M., Worsnop, D. R., Bäck, J., Petäjä, T., Kerminen, V.-M. and Kulmala, M.:  
623 Solar eclipse demonstrating the importance of photochemistry in new particle formation., *Sci. Rep.*, 7,  
624 45707, doi:10.1038/srep45707, 2017.

625 Jokinen, T., Sipilä, M., Kontkanen, J., Vakkari, V., Tisler, P., Duplissy, E. M., Junninen, H., Kangasluoma,  
626 J., Manninen, H. E., Petäjä, T., Kulmala, M., Worsnop, D. R., Kirkby, J., Virkkula, A. and Kerminen, V. M.:  
627 Ion-induced sulfuric acid–ammonia nucleation drives particle formation in coastal Antarctica, , 4(11),  
628 eaat9744, doi:10.1126/SCIADV.AAT9744, 2018.

629 Junninen, H., Ehn, M., Petäjä, T., Luosujärvi, L., Kotiaho, T., Kostianen, R., Rohner, U., Gonin, M., Fuhrer,  
630 K., Kulmala, M. and Worsnop, D. R.: A high-resolution mass spectrometer to measure atmospheric ion  
631 composition, *Atmos. Meas. Tech.*, 3(4), 1039–1053, doi:10.5194/amt-3-1039-2010, 2010.

632 Kalnay, E., Kanamitsu, M., Kistler, R., Collins, W., Deaven, D., Gandin, L. and E. Kalnay M. Kanamitsu R.  
633 Kistler W. Collins D. Deaven L. Gandin M. Iredell S. Saha G. White J. Woollen Y. Zhu M. Chelliah W.  
634 Ebisuzaki W. HE. Kalnay M. Kanamitsu R. Kistler W. Collins D. Deaven L. Gandin M. Iredell S. Saha G.  
635 White, and D. J.: The NCEP/NCAR 40-Year Reanalysis Project, *Bull. Am. Meteorol. Soc.*, 437–472,  
636 doi:[https://doi.org/10.1175/1520-0477\(1996\)077<0437:TNYRP>2.0.CO;2](https://doi.org/10.1175/1520-0477(1996)077<0437:TNYRP>2.0.CO;2), 1996.

637 Kempainen, J., Niittynen, P., Virkkala, A.-M., Happonen, K., Riihimäki, H., Aalto, J. and Luoto, M.: Dwarf  
638 Shrubs Impact Tundra Soils: Drier, Colder, and Less Organic Carbon, *Ecosyst.* 2021, 1–15,  
639 doi:10.1007/S10021-020-00589-2, 2021.

640 Kerminen, V.-M., Paramonov, M., Anttila, T., Riipinen, I., Fountoukis, C., Korhonen, H., Asmi, E., Laakso,  
641 L., Lihavainen, H., Swietlicki, E., Svenningsson, B., Asmi, A., Pandis, S. N., Kulmala, M. and Petäjä, T.:  
642 Cloud condensation nuclei production associated with atmospheric nucleation: a synthesis based on existing  
643 literature and new results, *Atmos. Chem. Phys.*, 12(24), 12037–12059, doi:10.5194/acp-12-12037-2012,  
644 2012.

645 Kerminen, V., Aurela, M., Hillamo, R. E. and Virkkula, A.: Formation of particulate MSA: deductions from  
646 size distribution measurements in the Finnish Arctic, *Tellus B*, 49(2), 159–171, doi:10.1034/j.1600-  
647 0889.49.issue2.4.x, 1997.

648 Kirkby, J., Curtius, J., Almeida, J., Dunne, E., Duplissy, J., Ehrhart, S., Franchin, A., Gagné, S., Ickes, L.,  
649 Kürten, A., Kupc, A., Metzger, A., Riccobono, F., Rondo, L., Schobesberger, S., Tsagkogeorgas, G.,  
650 Wimmer, D., Amorim, A., Bianchi, F., Breitenlechner, M., David, A., Dommen, J., Downard, A., Ehn, M.,

- 651 Flagan, R. C., Haider, S., Hansel, A., Hauser, D., Jud, W., Junninen, H., Kreissl, F., Kvashin, A., Laaksonen,  
652 A., Lehtipalo, K., Lima, J., Lovejoy, E. R., Makhmutov, V., Mathot, S., Mikkilä, J., Minginette, P., Mogo,  
653 S., Nieminen, T., Onnela, A., Pereira, P., Petäjä, T., Schnitzhofer, R., Seinfeld, J. H., Sipilä, M., Stozhkov,  
654 Y., Stratmann, F., Tomé, A., Vanhanen, J., Viisanen, Y., Vrtala, A., Wagner, P. E., Walther, H.,  
655 Weingartner, E., Wex, H., Winkler, P. M., Carslaw, K. S., Worsnop, D. R., Baltensperger, U. and Kulmala,  
656 M.: Role of sulphuric acid, ammonia and galactic cosmic rays in atmospheric aerosol nucleation., *Nature*,  
657 476(7361), 429–433, doi:10.1038/nature10343, 2011.
- 658 Kirkby, J., Duplissy, J., Sengupta, K., Frege, C., Gordon, H., Williamson, C., Heinritzi, M., Simon, M., Yan,  
659 C., Almeida, J. J., Trostl, J., Nieminen, T., Ortega, I. K., Wagner, R., Adamov, A., Amorim, A.,  
660 Bernhammer, A.-K. K., Bianchi, F., Breitenlechner, M., Brilke, S., Chen, X., Craven, J., Dias, A., Ehrhart,  
661 S., Flagan, R. C., Franchin, A., Fuchs, C., Guida, R., Hakala, J., Hoyle, C. R., Jokinen, T., Junninen, H.,  
662 Kangasluoma, J., Kim, J., Krapf, M., Kurten, A., Laaksonen, A., Lehtipalo, K., Makhmutov, V., Mathot, S.,  
663 Molteni, U., Onnela, A., Perakyla, O., Piel, F., Petaja, T., Praplan, A. P., Pringle, K., Rap, A., Richards, N.  
664 A. D. D., Riipinen, I., Rissanen, M. P., Rondo, L., Sarnela, N., Schobesberger, S., Scott, C. E., Seinfeld, J.  
665 H., Sipilä, M., Steiner, G., Stozhkov, Y., Stratmann, F., Tomé, A., Virtanen, A., Vogel, A. L., Wagner, A. C.,  
666 Wagner, P. E., Weingartner, E., Wimmer, D., Winkler, P. M., Ye, P., Zhang, X., Hansel, A., Dommen, J.,  
667 Donahue, N. M., Worsnop, D. R., Baltensperger, U., Kulmala, M., Carslaw, K. S., Curtius, J., Tröstl, J.,  
668 Nieminen, T., Ortega, I. K., Wagner, R., Adamov, A., Amorim, A., Bernhammer, A.-K. K., Bianchi, F.,  
669 Breitenlechner, M., Brilke, S., Chen, X., Craven, J., Dias, A., Ehrhart, S., Flagan, R. C., Franchin, A., Fuchs,  
670 C., Guida, R., Hakala, J., Hoyle, C. R., Jokinen, T., et al.: Ion-induced nucleation of pure biogenic particles,  
671 *Nature*, 533(7604), 521–526, doi:10.1038/nature17953, 2016.
- 672 Kulmala, M., Toivonen, A., Mäkelä, J. M. and Laaksonen, A.: Analysis of the growth of nucleation mode  
673 particles observed in Boreal forest, *Tellus B*, 50(5), 449–462, doi:10.1034/j.1600-0889.1998.t01-4-00004.x,  
674 1998.
- 675 Kulmala, M., Riipinen, I., Sipilä, M., Manninen, H. E., Petäjä, T., Junninen, H., Dal Maso, M., Mordas, G.,  
676 Mirme, A., Vana, M., Hirsikko, A., Laakso, L., Harrison, R. M., Hanson, I., Leung, C., Lehtinen, K. E. J. and  
677 Kerminen, V. M.: Toward direct measurement of atmospheric nucleation, *Science* (80-. ), 318(5847), 89–92,  
678 2007.
- 679 Kulmala, M., Kontkanen, J., Junninen, H., Lehtipalo, K., Manninen, H. E., Nieminen, T., Petäjä, T., Sipilä,  
680 M., Schobesberger, S., Rantala, P., Franchin, A., Jokinen, T., Järvinen, E., Äijälä, M., Kangasluoma, J.,  
681 Hakala, J., Aalto, P. P., Paasonen, P., Mikkilä, J., Vanhanen, J., Aalto, J., Hakola, H., Makkonen, U.,  
682 Ruuskanen, T., Mauldin, R. L., Duplissy, J., Vehkamäki, H., Bäck, J., Kortelainen, A., Riipinen, I., Kurtén,  
683 T., Johnston, M. V., Smith, J. N., Ehn, M., Mentel, T. F., Lehtinen, K. E. J. J., Laaksonen, A., Kerminen, V.-  
684 M. M. V.-M., Worsnop, D. R., Petaja, T., Sipilä, M., Schobesberger, S., Rantala, P., Franchin, A., Jokinen,  
685 T., Jarvinen, E., Aijala, M., Kangasluoma, J., Hakala, J., Aalto, P. P., Paasonen, P., Mikkilä, J., Vanhanen, J.,  
686 Aalto, J., Hakola, H., Makkonen, U., Ruuskanen, T., Mauldin, R. L., Duplissy, J., Vehkamäki, H., Back, J.,  
687 Kortelainen, A., Riipinen, I., Kurten, T., Johnston, M. V., Smith, J. N., Ehn, M., Mentel, T. F., Lehtinen, K.  
688 E. J. J., Laaksonen, A., Kerminen, V.-M. M. V.-M., Worsnop, D. R., Petäjä, T., Sipilä, M., Schobesberger,  
689 S., Rantala, P., Franchin, A., Jokinen, T., Järvinen, E., Äijälä, M., Kangasluoma, J., Hakala, J., Aalto, P. P.,  
690 Paasonen, P., Mikkilä, J., Vanhanen, J., Aalto, J., Hakola, H., Makkonen, U., Ruuskanen, T., Mauldin, R. L.,  
691 Duplissy, J., Vehkamäki, H., Bäck, J., Kortelainen, A., Riipinen, I., Kurtén, T., Johnston, M. V., Smith, J. N.,  
692 et al.: Direct observations of atmospheric aerosol nucleation., *Science*, 339(6122), 943–6,  
693 doi:10.1126/science.1227385, 2013.
- 694 Kulmala, M., Ezhova, E., Kalliokoski, T., Noe, S., Vesala, T., Lohila, A., Liski, J., Makkonen, R., Bäck, J.,  
695 Petäjä, T. and Kerminen, V.-M.: CarbonSink+-Accounting for multiple climate feedbacks from forests,  
696 *Boreal Environ. Res.*, 25, 145-159, 2020.
- 697 Kürten, A., Rondo, L., Ehrhart, S. and Curtius, J.: Calibration of a chemical ionization mass spectrometer for  
698 the measurement of gaseous sulfuric acid, *J. Phys. Chem. A*, 116(24), 6375–6386, doi:10.1021/jp212123n,  
699 2012.
- 700 Kürten, A., Jokinen, T., Simon, M., Sipilä, M., Sarnela, N., Junninen, H., Adamov, A., Almeida, J., Amorim,

701 A., Bianchi, F., Breitenlechner, M., Dommen, J., Donahue, N. M., Duplissy, J., Ehrhart, S., Flagan, R. C.,  
702 Franchin, A., Hakala, J., Hansel, A., Heinritzi, M., Hutterli, M., Kangasluoma, J., Kirkby, J., Laaksonen, A.,  
703 Lehtipalo, K., Leiminger, M., Makhmutov, V., Mathot, S., Onnela, A., Petäjä, T., Praplan, A. P., Riccobono,  
704 F., Rissanen, M. P., Rondo, L., Schobesberger, S., Seinfeld, J. H., Steiner, G., Tomé, A., Tröstl, J., Winkler,  
705 P. M., Williamson, C., Wimmer, D., Ye, P., Baltensperger, U., Carslaw, K. S., Kulmala, M., Worsnop, D. R.,  
706 Curtius, J. and Barbara Finlayson-Pitts, by J.: Neutral molecular cluster formation of sulfuric acid–  
707 dimethylamine observed in real time under atmospheric conditions, *Proc. Natl. Acad. Sci. U.S.A.*, 111(42),  
708 15019–15024, doi:10.1073/pnas.1404853111, 2014.

709 Kyrö, E. M., Väänänen, R., Kerminen, V. M., Virkkula, A., Petäjä, T., Asmi, A., Dal Maso, M., Nieminen,  
710 T., Juhola, S., Shcherbinin, A., Riipinen, I., Lehtipalo, K., Keronen, P., Aalto, P. P., Hari, P. and Kulmala,  
711 M.: Trends in new particle formation in eastern Lapland, Finland: Effect of decreasing sulfur emissions from  
712 Kola Peninsula, *Atmos. Chem. Phys.*, 14(9), 4383–4396, 2014.

713 Lai, S. C., Williams, J., Arnold, S. R., Atlas, E. L., Gebhardt, S. and Hoffmann, T.: Iodine containing species  
714 in the remote marine boundary layer: A link to oceanic phytoplankton, *Geophys. Res. Lett.*, 38(20),  
715 doi:10.1029/2011GL049035, 2011.

716 Lehtipalo, K., Yan, C., Dada, L., Bianchi, F., Xiao, M., Wagner, R., Stolzenburg, D., Ahonen, L. R.,  
717 Amorim, A., Baccarini, A., Bauer, P. S., Baumgartner, B., Bergen, A., Bernhammer, A.-K., Breitenlechner,  
718 M., Brilke, S., Buchholz, A., Mazon, S. B., Chen, D., Chen, X., Dias, A., Dommen, J., Draper, D. C.,  
719 Duplissy, J., Ehn, M., Finkenzeller, H., Fischer, L., Frege, C., Fuchs, C., Garmash, O., Gordon, H., Hakala,  
720 J., He, X., Heikkinen, L., Heinritzi, M., Helm, J. C., Hofbauer, V., Hoyle, C. R., Jokinen, T., Kangasluoma,  
721 J., Kerminen, V.-M., Kim, C., Kirkby, J., Kontkanen, J., Kürten, A., Lawler, M. J., Mai, H., Mathot, S.,  
722 Mauldin, R. L., Molteni, U., Nichman, L., Nie, W., Nieminen, T., Ojdanic, A., Onnela, A., Passananti, M.,  
723 Petäjä, T., Piel, F., Pospisilova, V., Quéléver, L. L. J., Rissanen, M. P., Rose, C., Sarnela, N., Schallhart, S.,  
724 Schuchmann, S., Sengupta, K., Simon, M., Sipilä, M., Tauber, C., Tomé, A., Tröstl, J., Väisänen, O., Vogel,  
725 A. L., Volkamer, R., Wagner, A. C., Wang, M., Weitz, L., Wimmer, D., Ye, P., Ylisirniö, A., Zha, Q.,  
726 Carslaw, K. S., Curtius, J., Donahue, N. M., Flagan, R. C., Hansel, A., Riipinen, I., Virtanen, A., Winkler, P.  
727 M., Baltensperger, U., Kulmala, M. and Worsnop, D. R.: Multicomponent new particle formation from  
728 sulfuric acid, ammonia, and biogenic vapors, *Sci. Adv.*, 4(12), eaau5363, doi:10.1126/sciadv.aau5363, 2018.

729 Leino, K., Nieminen, T., Manninen, H. E., Petäjä, T., Kerminen, V.-M. and Kulmala, M.: Intermediate ions  
730 as a strong indicator of new particle formation bursts in a boreal forest, *Boreal Environ. Res.*, 21(3-4), 274-  
731 286, 2016.

732 Lévassieur, M.: Impact of Arctic meltdown on the microbial cycling of sulphur., *Nat. Geosci.*, 6(9), 691-700,  
733 2013.

734 Mäkelä, J. M., Aalto, P., Jokinen, V., Pohja, T., Nissinen, A., Palmroth, S., Markkanen, T., Seitsonen, K.,  
735 Lihavainen, H. and Kulmala, M.: Observations of ultrafine aerosol particle formation and growth in boreal  
736 forest, *Geophys. Res. Lett.*, 24(10), 1219–1222, doi:10.1029/97GL00920, 1997.

737 Manninen, H. E., Mirme, S., Mirme, A., Petäjä, T. and Kulmala, M.: How to reliably detect molecular  
738 clusters and nucleation mode particles with Neutral cluster and Air Ion Spectrometer (NAIS), *Atmos. Meas.*  
739 *Tech.*, 9(8), 3577–3605, 2016.

740 Maso, M. D., Dal Maso, M., Kulmala, M., Riipinen, I., Wagner, R., Hussein, T., Aalto, P. P. and Lehtinen,  
741 K. E. J.: Formation and growth of fresh atmospheric aerosols: Eight years of aerosol size distribution data  
742 from SMEAR II, Hyytiälä, Finland, *Boreal Environ. Res.*, 10(5), 323–336, 2005.

743 Mauldin, R., Kosciuch, E., Eisele, F., Huey, G., Tanner, D., Sjostedt, S., Blake, D., Chen, G., Crawford, J.  
744 and Davis, D.: South Pole Antarctica observations and modeling results: New insights on HO<sub>x</sub> radical and  
745 sulfur chemistry, *Atmos. Environ.*, 44(4), 572–581, doi:10.1016/j.atmosenv.2009.07.058, 2010.

746 Mauldin, R. L., Kosciuch, E., Henry, B., Eisele, F. L., Shetter, R., Lefer, B., Chen, G., Davis, D., Huey, G.  
747 and Tanner, D.: Measurements of OH, HO<sub>2</sub>+RO<sub>2</sub>, H<sub>2</sub>SO<sub>4</sub>, and MSA at the South Pole during ISCAT 2000,  
748 *Atmos. Environ.*, 38(32), 5423–5437, doi:10.1016/j.atmosenv.2004.06.031, 2004.

749 McFiggans, G., Bale, C. S. E. E., Ball, S. M., Beames, J. M., Bloss, W. J., Carpenter, L. J., Dorsey, J., Dunk,  
750 R., Flynn, M. J., Furneaux, K. L., Gallagher, M. W., Heard, D. E., Hollingsworth, A. M., Hornsby, K.,  
751 Ingham, T., Jones, C. E., Jones, R. L., Kramer, L. J., Langridge, J. M., Leblanc, C., LeCrane, J. P.-P., Lee, J.  
752 D., Leigh, R. J., Longley, I., Mahajan, A. S., Monks, P. S., Oetjen, H., Orr-Ewing, a. J., Plane, J. M. C. C.,  
753 Potin, P., Shillings, a. J. L. L., Thomas, F., Von Glasow, R., Wada, R., Whalley, L. K. and Whitehead, J. D.:  
754 Iodine-mediated coastal particle formation: an overview of the Reactive Halogens in the Marine Boundary  
755 Layer (RHAMBLe) Roscoff coastal study, *Atmos. Chem. Phys.*, 10(6), 2975–2999, doi:10.5194/acpd-9-  
756 26421-2009, 2010.

757 Mirme, S. and Mirme, A.: The mathematical principles and design of the NAIS – a spectrometer for the  
758 measurement of cluster ion and nanometer aerosol size distributions, *Atmos. Meas. Tech.*, 6(4), 1061–1071,  
759 doi:10.5194/amt-6-1061-2013, 2013.

760 Myllys, N., Ponkkonen, T., Passananti, M., Elm, J., Vehkamäki, H. and Olenius, T.: Guanidine: A Highly  
761 Efficient Stabilizer in Atmospheric New-Particle Formation, *J. Phys. Chem. A*, 122(20), 4717–4729,  
762 doi:10.1021/acs.jpca.8b02507, 2018.

763 Napari, I., Noppel, M., Vehkamäki, H. and Kulmala, M.: Parametrization of ternary nucleation rates for  
764 H<sub>2</sub>SO<sub>4</sub>-NH<sub>3</sub>-H<sub>2</sub>O vapors, *J. Geophys. Res. Atmos.*, 107(19), AAC 6-1-AAC 6-6,  
765 doi:10.1029/2002JD002132, 2002.

766 Nieminen, T., Asmi, A., Maso, M. D., Aalto, P. P., Keronen, P., Kulmala, M., Kerminen, V., Dal maso, M.,  
767 Aalto, P. P., Keronen, P., Petäjä, T., Kulmala, M. and Kerminen, V.: Trends in atmospheric new-particle  
768 formation: 16 years of observations in a boreal-forest environment, *Boreal Environ. Res.*, 19 (suppl.(2004)),  
769 191–214, 2014.

770 O’Dowd, C. D., Jimenez, J. L., Bahreini, R., Flagan, R. C., Seinfeld, J. H., Hämerl, K., Pirjola, L., Kulmala,  
771 M. and Hoffmann, T.: Marine aerosol formation from biogenic iodine emissions, *Nature*, 417(6889), 632–  
772 636, 2002.

773 Paasonen, P., Asmi, A., Petäjä, T., Kajos, M. K., Äijälä, M., Junninen, H., Holst, T., Abbatt, J. P. D. D.,  
774 Arneth, A., Birmili, W., Van Der Gon, H. D., Hamed, A., Hoffer, A., Laakso, L., Laaksonen, A., Richard  
775 Leaitch, W., Plass-Dülmer, C., Pryor, S. C., Räisänen, P., Swietlicki, E., Wiedensohler, A., Worsnop, D. R.,  
776 Kerminen, V.-M. M. and Kulmala, M.: Warming-induced increase in aerosol number concentration likely to  
777 moderate climate change, *Nat. Geosci.*, 6(6), 438–442, doi:10.1038/ngeo1800, 2013.

778 Park, K., Lee, K., Kim, T., Yoon, Y. J., Jang, E., Jang, S., Lee, B. and Hermansen, O.: Atmospheric DMS in  
779 the Arctic Ocean and Its Relation to Phytoplankton Biomass, *Global Biogeochem. Cycles*, 32(3), 351–359,  
780 doi:10.1002/2017GB005805, 2018.

781 Pirjola, L., Laaksonen, A., Aalto, P. and Kulmala, M.: Sulfate aerosol formation in the Arctic boundary  
782 layer, *J. Geophys. Res. Atmos.*, 103(D7), 8309–8321, doi:10.1029/97JD03079, 1998.

783 Raso, A. R. W., Custard, K. D., May, N. W., Tanner, D., Newburn, M. K., Walker, L., Moore, R. J., Huey,  
784 L. G., Alexander, L., Shepson, P. B. and Pratt, K. A.: Active molecular iodine photochemistry in the Arctic,  
785 *Proc. Natl. Acad. Sci. U. S. A.*, 114(38), 10053–10058, doi:10.1073/pnas.1702803114, 2017.

786 Reyer, C. P. O., Brouwers, N., Rammig, A., Brook, B. W., Epila, J., Grant, R. F., Holmgren, M.,  
787 Langerwisch, F., Leuzinger, S., Lucht, W., Medlyn, B., Pfeifer, M., Steinkamp, J., Vanderwel, M. C.,  
788 Verbeeck, H. and Vilella, D. M.: Forest resilience and tipping points at different spatio-temporal scales:  
789 Approaches and challenges, *J. Ecol.*, 103(1), 5–15, doi:10.1111/1365-2745.12337, 2015.

790 Riva, M., Rantala, P., Krechmer, E. J., Peräkylä, O., Zhang, Y., Heikkinen, L., Garmash, O., Yan, C.,  
791 Kulmala, M., Worsnop, D. and Ehn, M.: Evaluating the performance of five different chemical ionization  
792 techniques for detecting gaseous oxygenated organic species, *Atmos. Meas. Tech.*, 12(4), 2403–2421,  
793 doi:10.5194/amt-12-2403-2019, 2019.

794 Ruuskanen, T., Reissell, M., Keronen, A., Aalto, P. P., Laakso, P. P., Grönholm, L., Hari, T. and Kulmala,  
795 P.: Atmospheric trace gas and aerosol particle concentration measurements in Eastern Lapland, *Boreal Env.*

796 Res, 8(4), 335-349, 2003.

797 Ruuskanen, T. M., Kaasik, M., Aalto, P. P., Hörrak, U., Vana, M., Mårtensson, M., Yoon, Y. J., Keronen, P.,  
798 Mordas, G., Ceburnis, D., Nilsson, E. D., O'Dowd, C., Noppel, M., Alliksaar, T., Ivask, J., Sofiev, M.,  
799 Prank, M. and Kulmala, M.: Concentrations and fluxes of aerosol particles during the LAPBIAT  
800 measurement campaign at Värriö field station, *Atmos. Chem. Phys.*, 7(14), 3683–3700, doi:10.5194/acp-7-  
801 3683-2007, 2007.

802 Schmale, J., Zieger, P. and Ekman, A. M. L.: Aerosols in current and future Arctic climate, *Nat. Clim.*  
803 *Chang.*, 11(2), 95–105, doi:10.1038/s41558-020-00969-5, 2021.

804 Seco, R., Holst, T., Sillesen Matzen, M., Westergaard-Nielsen, A., Li, T., Simin, T., Jansen, J., Crill, P.,  
805 Friborg, T., Rinne, J. and Rinnan, R.: Volatile organic compound fluxes in a subarctic peatland and lake,  
806 *Atmos. Chem. Phys.*, 20(21), 13399–13416, doi:10.5194/ACP-20-13399-2020, 2020.

807 Sherwen, T. M., Evans, M. J., Spracklen, D. V., Carpenter, L. J., Chance, R., Baker, A. R., Schmidt, J. A.  
808 and Breider, T. J.: Global modeling of tropospheric iodine aerosol, *Geophys. Res. Lett.*, 43(18), 10012–  
809 10019, doi:10.1002/2016gl070062, 2016.

810 Sipilä, M., Sarnela, N., Jokinen, T., Henschel, H., Junninen, H., Kontkanen, J., Richters, S., Kangasluoma, J.,  
811 Franchin, A., Peräkylä, O., Rissanen, M. P., Ehn, M., Vehkamäki, H., Kurten, T., Berndt, T., Petäjä, T.,  
812 Worsnop, D., Ceburnis, D., Kerminen, V.-M. M., Kulmala, M., O'Dowd, C. and O'Dowd, C.: Molecular-  
813 scale evidence of aerosol particle formation via sequential addition of HIO<sub>3</sub>, *Nature*, 537(7621), 532–534,  
814 doi:10.1038/nature19314, 2016.

815 Sipilä, M., Sarnela, N., Neitola, K., Laitinen, T., Kemppainen, D., Beck, L., Duplissy, E.-M., Kuittinen, S.,  
816 Lehmusjärvi, T., Lampilahti, J., Kerminen, V.-M., Lehtipalo, K., Aalto, P., Keronen, P., Siivola, E., Rantala,  
817 P., Worsnop, D., Kulmala, M., Jokinen, T. and Petäjä, T.: Wintertime sub-arctic new particle formation from  
818 Kola Peninsula sulphur emissions, *Atmos. Chem. Phys.*, 21(23), 17559–17576,  
819 doi:https://doi.org/10.5194/acp-21-17559-2021, 2021.

820 Sive, B. C., Varner, R. K., Mao, H., Blake, D. R., Wingenter, O. W. and Talbot, R.: A large terrestrial source  
821 of methyl iodide, *Geophys. Res. Lett.*, 34(17), L17808, doi:10.1029/2007gl030528, 2007.

822 Spolaor, A., Barbaro, E., Cappelletti, D., Turetta, C., Mazzola, M., Giardi, F., Björkman, M., Lucchetta, F.,  
823 Dallo, F., Pfaffhuber, K. A., Angot, H., Dommergue, A., Maturilli, M., Saiz-Lopez, A., Barbante, C. and  
824 Cairns, W.: Diurnal cycle of iodine and mercury concentrations in Svalbard surface snow, *Atmos. Chem.*  
825 *Phys. Discuss.*, 1–25, doi:10.5194/ACP-2019-285, 2019.

826 Stohl, A.: Characteristics of atmospheric transport into the Arctic troposphere, *J. Geophys. Res. Atmos.*, 111,  
827 D11306, doi:10.1029/2005JD006888, 2006.

828 Sulo, J., Sarnela, N., Kontkanen, J., Ahonen, L., Paasonen, P., Laurila, T., Jokinen, T., Kangasluoma, J.,  
829 Junninen, H., Sipilä, M., Petäjä, T., Kulmala, M. and Lehtipalo, K.: Long-term measurement of sub-  
830 3&thinsp;nm particles and their precursor gases in the boreal forest, *Atmos. Chem. Phys.*, 21(2), 695–715,  
831 doi:10.5194/acp-21-695-2021, 2021.

832 Tarvainen, V., Hakola, H., Hellén, H., Bäck, J., Hari, P. and Kulmala, M.: Temperature and light dependence  
833 of the VOC emissions of Scots pine, *Atmos. Chem. Phys.*, 4(5), 989-998, doi: 10.5194/acp-5-989-2005,  
834 2004.

835 Tiiva, P., Faubert, P., Michelsen, A., Holopainen, T., Holopainen, J. K. and Rinnan, R.: Climatic warming  
836 increases isoprene emission from a subarctic heath, *New Phytol.*, 180(4), 853–863, doi:10.1111/J.1469-  
837 8137.2008.02587.X, 2008.

838 Tunved, P., Hansson, H. C., Kerminen, V. M., Ström, J., Dal Maso, M., Lihavainen, H., Viisanen, Y., Aalto,  
839 P. P., Komppula, M. and Kulmala, M.: High natural aerosol loading over boreal forests, *Science (80-. )*,  
840 312(5771), 261–263, doi:10.1126/science.1123052, 2006.

841 Valolahti, H., Kivimäenpää, M., Faubert, P., Michelsen, A. and Rinnan, R.: Climate change-induced



842 vegetation change as a driver of increased subarctic biogenic volatile organic compound emissions, *Glob.*  
843 *Chang. Biol.*, 21(9), 3478–3488, doi:10.1111/GCB.12953, 2015.

844 Vana, M., Komsaare, K., Hörrak, U., Mirme, S., Nieminen, T., Kontkanen, J., Manninen, H. E., Petäjä, T.,  
845 Noe, S. M. and Kulmala, M.: Characteristics of new-particle formation at three SMEAR stations, *Boreal*  
846 *Environ. Res.*, 21(3-4), 345-362, 2016.

847 Vehkamäki, H., Dal Maso, M., Hussein, T., Flanagan, R., Hyvärinen, A., Lauros, J., Merikanto, J.,  
848 Mönkkönen, P., Pihlatie, M., Salminen, K., Sogacheva, L., Thum, T., Ruuskanen, T. M., Keronen, P., Aalto,  
849 P. P., Hari, P., Lehtinen, K. E. J., Rannik, Ü. and Kulmala, M.: Atmospheric particle formation events at  
850 Värriö measurement station in Finnish Lapland 1998-2002, *Atmos. Chem. Phys.*, 4(7), 2015–2023,  
851 doi:10.5194/acp-4-2015-2004, 2004.

852 Wang, S., Riva, M., Yan, C., Ehn, M. and Wang, L.: Primary Formation of Highly Oxidized Multifunctional  
853 Products in the OH-Initiated Oxidation of Isoprene: A Combined Theoretical and Experimental Study,  
854 *Environ. Sci. Technol.*, 52(21), 12255–12264, doi:10.1021/acs.est.8b02783, 2018.

855 Wang, Y. Q., Zhang, X. Y. and Draxler, R. R.: TrajStat: GIS-based software that uses various trajectory  
856 statistical analysis methods to identify potential sources from long-term air pollution measurement data,  
857 *Environ. Model. Softw.*, 24(8), 938–939, doi:10.1016/j.envsoft.2009.01.004, 2009.

858 Yan, C., Nie, W., Äijälä, M., Rissanen, M. P., Canagaratna, M. R., Massoli, P., Junninen, H., Jokinen, T.,  
859 Sarnela, N., Häme, S. A. K. K., Schobesberger, S., Canonaco, F., Yao, L., Prévôt, A. S. H. H., Petäjä, T.,  
860 Kulmala, M., Sipilä, M., Worsnop, D. R., Ehn, M., Äijälä, M., Rissanen, M. P., Canagaratna, M. R., Massoli,  
861 P., Junninen, H., Jokinen, T., Sarnela, N., Häme, S. A. K. K., Schobesberger, S., Canonaco, F., Yao, L.,  
862 Prévôt, A. S. H. H., Petäjä, T., Kulmala, M., Sipilä, M., Worsnop, D. R. and Ehn, M.: Source  
863 characterization of highly oxidized multifunctional compounds in a boreal forest environment using positive  
864 matrix factorization, *Atmos. Chem. Phys.*, 16(19), 12715–12731, doi:10.5194/acp-16-12715-2016, 2016.

865 Yu, H., Ren, L., Huang, X., Xie, M., He, J. and Xiao, H.: Iodine speciation and size distribution in ambient  
866 aerosols at a coastal new particle formation hotspot in China, *Atmos. Chem. Phys.*, 19(6), 4025–4039,  
867 doi:10.5194/acp-19-4025-2019, 2019.

868